

Rate-Dependent Homogenization based Continuum Plasticity  
Damage Model for Dendritic Cast Aluminum Alloys

A Thesis

Presented in Partial Fulfillment of the Requirements for  
the Degree Master of Science in the  
Graduate School of The Ohio State University

By

Piyush Prashant Dondeti, B.E.  
Graduate Program in Mechanical Engineering

\* \* \* \* \*

The Ohio State University

2011

Master's Examination Committee:

Prof. Somnath Ghosh, Adviser

Prof. June K. Lee

# Report Documentation Page

Form Approved  
OMB No. 0704-0188

Public reporting burden for the collection of information is estimated to average 1 hour per response, including the time for reviewing instructions, searching existing data sources, gathering and maintaining the data needed, and completing and reviewing the collection of information. Send comments regarding this burden estimate or any other aspect of this collection of information, including suggestions for reducing this burden, to Washington Headquarters Services, Directorate for Information Operations and Reports, 1215 Jefferson Davis Highway, Suite 1204, Arlington VA 22202-4302. Respondents should be aware that notwithstanding any other provision of law, no person shall be subject to a penalty for failing to comply with a collection of information if it does not display a currently valid OMB control number.

1. REPORT DATE <b>JUL 2011</b>		2. REPORT TYPE		3. DATES COVERED <b>00-00-2011 to 00-00-2011</b>	
4. TITLE AND SUBTITLE <b>Rate-Dependent Homogenization Based Continuum Plasticity Damage Model For Dendritic Cast Aluminum Alloys</b>				5a. CONTRACT NUMBER	
				5b. GRANT NUMBER	
				5c. PROGRAM ELEMENT NUMBER	
6. AUTHOR(S)				5d. PROJECT NUMBER	
				5e. TASK NUMBER	
				5f. WORK UNIT NUMBER	
7. PERFORMING ORGANIZATION NAME(S) AND ADDRESS(ES) <b>The Ohio State University, Columbus, OH, 43210</b>				8. PERFORMING ORGANIZATION REPORT NUMBER	
9. SPONSORING/MONITORING AGENCY NAME(S) AND ADDRESS(ES)				10. SPONSOR/MONITOR'S ACRONYM(S)	
				11. SPONSOR/MONITOR'S REPORT NUMBER(S)	
12. DISTRIBUTION/AVAILABILITY STATEMENT <b>Approved for public release; distribution unlimited</b>					
13. SUPPLEMENTARY NOTES					
14. ABSTRACT					
15. SUBJECT TERMS					
16. SECURITY CLASSIFICATION OF:			17. LIMITATION OF ABSTRACT	18. NUMBER OF PAGES	19a. NAME OF RESPONSIBLE PERSON
a. REPORT <b>unclassified</b>	b. ABSTRACT <b>unclassified</b>	c. THIS PAGE <b>unclassified</b>			

© Copyright by  
Piyush Prashant Dondeti  
2011

## ABSTRACT

The objective of this dissertation is to develop a computationally efficient rate-dependent homogenization based continuum plasticity damage model for macroscopic analysis of ductile failure in porous ductile materials containing brittle inclusions. The macroscopic model developed in this dissertation is an extension of the model proposed by Ghosh et al. [S. Ghosh, J. Bai, and D. Paquet. Homogenization-based continuum plasticity damage model for ductile failure of materials containing heterogeneities. *J Mech Phys Solids*, 57:10171044, 2009]. The overall framework of this rate-dependent HCPD model follows the structure of the anisotropic Gursen-Tvergaard-Needleman(GTN) type elasto-plasticity model for porous ductile materials. This model is assumed to be orthotropic in an evolving material principal coordinate system throughout deformation history. The viscoplastic behavior is modeled through an over-stress viscoplastic model. Anisotropy and viscoplastic parameters in the rate-dependent HCPD model are calibrated from homogenization of evolving micro-variables in representative volume element (RVE) of the microstructure. These parameters are dependent on microstructural features such as morphology and distribution of different phases. Micromechanical analyses for this purpose are performed by locally enhanced Voronoi cell finite element model (LE-VCFEM) [Hu, C., Ghosh, S., 2008. Locally enhanced Voronoi cell finite element model for simulating evolving fracture in ductile microstructures containing inclusions. *Int. J. Numer.*

Methods Eng. 76(12),1955-1992]. This work also introduces a novel rate-dependent void nucleation criterion for the macroscopic damage evolution due to the combined inclusion and matrix cracking happening in the underlying microstructure of the RVE. The results of the rate-dependent HCPD model are compared with the homogenized micromechanics (LE-VCFEM) results and show excellent agreement.

*Dedicated to my family and friends.*

## ACKNOWLEDGMENTS

I would like to begin by acknowledging my advisor and mentor, Professor Somnath Ghosh, for giving me this wonderful opportunity to learn from him. I thank him for his patience and guidance during the course of my research. I would also like to acknowledge Professor June K. Lee for being on my thesis defense committee and for his valuable help during my defense.

This work has been supported by the National Science Foundation NSF Div Civil and Mechanical Systems Division through the GOALI Grant No. CMS-0308666 (Program Director: Dr. G. Paulino), by the Department of Energy Aluminum Visions program through Grant No. A5997 and by the Army Research Office through Grant No. DAAD19-02-1-0428 (Program Director: Dr. B. Lamattina). This sponsorship is gratefully acknowledged. The author is grateful to Drs. Steve Harris, John Allison, Xuming Su, and James Boileau of Ford Research Laboratory for invaluable discussions and for micrographs, samples and data used in this paper. Computer support by the Ohio Supercomputer Center through Grant PAS813-2 is also gratefully acknowledged.

This work would not have been possible without the help of my labmate Daniel throughout my research. I would also like to thank all other lab members, especially Prabu, Pritam, Adarsh, and Masoud for the wonderful times during the past two years.

## VITA

June 2008 ..... (B.E.) College of Engineering, Anna University, Chennai, India  
June 2009 - Present ..... Graduate Research Associate, Computational Mechanics Research Lab, The Ohio State University

## PUBLICATIONS FROM THIS WORK

### Research Publications

“Dual-Stage Nested Homogenization for Rate-Dependent Anisotropic Elasto-Plasticity Model of Dendritic Cast Aluminum Alloys”, Daniel Paquet, **Piyush Dondeti** and Somnath Ghosh, *International Journal of Plasticity* (In Press).

## FIELDS OF STUDY

Major Field: Mechanical Engineering

# TABLE OF CONTENTS

	Page
Abstract . . . . .	ii
Dedication . . . . .	iv
Acknowledgments . . . . .	v
Vita . . . . .	vi
List of Tables . . . . .	ix
List of Figures . . . . .	x
Chapters:	
1. Introduction . . . . .	1
1.1 Literature Survey . . . . .	3
1.2 Thesis Overview . . . . .	4
2. Tools needed for developing the rate-dependent HCPD model . . . . .	5
2.1 Identification of the statistically equivalent RVE size . . . . .	5
2.2 Homogenization of micromechanical variables in RVE analysis . . .	12
2.3 Locally enhanced voronoi cell finite element model (LE-VCFEM) .	13
3. Rate-Dependent Homogenization Based Continuum Plasticity Damage Model	14
3.1 Evolving Anisotropy . . . . .	17
3.2 Rate-Dependent Void Nucleation Criterion . . . . .	18
3.3 Numerical implementation of the rate-dependent HCPD model . .	22

4.	Calibration of rate-dependent HCPD model parameters . . . . .	24
4.1	$Y_f(W_p)$ and $C$ in Equations (3.3, 3.11) . . . . .	24
4.2	Parameters $F, G$ and $H$ in equation (3.11) . . . . .	25
4.3	Viscoplastic parameters $\Gamma_0$ and $p$ in Equation (3.10) . . . . .	26
4.4	Parameters $Q_1$ and $Q_2$ in Equation (3.3) . . . . .	28
4.5	Calibration of parameters in the void nucleation model . . . . .	30
4.5.1	$\mathbf{e}_0$ and $m$ calibration . . . . .	30
4.5.2	A, B and C calibration . . . . .	33
5.	Numerical examples with the rate-dependent HCPD model . . . . .	37
5.1	Viscoplastic response and void growth model . . . . .	38
5.2	Void nucleation model . . . . .	39
5.3	Dual-stage nested homogenization . . . . .	44
6.	SUMMARY AND FUTURE WORK . . . . .	46
6.1	Summary . . . . .	46
6.2	Future Work . . . . .	47
	Bibliography . . . . .	48

## LIST OF TABLES

Table		Page
4.1	Mean and standard deviation of calibrated parameters $Q_1$ and $Q_2$ for different RVEs . . . . .	30
4.2	Values of anisotropy parameters $A, B$ and $C$ at different angles of principal strain $\theta_p$ . The value of $A(\theta_p = 0^\circ) = 1$ for all RVEs . . . .	36

## LIST OF FIGURES

Figure	Page
1.1 (a) Micrograph of a cast aluminum alloy AS7GU ( $120 \mu\text{m} \times 96 \mu\text{m}$ ), (b) blow-up of the designated region in (a) ( $28.4 \mu\text{m} \times 28.4 \mu\text{m}$ ). . .	2
2.1 (a) Marked correlation function for two different windows A and B using the mark of Equation (2.4), (b) radius of convergence $r_0$ based on the results of (a) as a function of the chosen tolerance. . . . .	9
2.2 (a) Micrograph of the microstructural domain of SERVE A, (b) mi- crograph of the microstructural domain of SERVE B, (c) SERVE A with periodic boundary, (d) SERVE B with periodic boundary. . . .	10
2.3 Hardening (stress-strain) curve for the aluminum matrix used for comparison of macroscopic behavior in shear for SERVE A and SERVE B of Figure 2.2. . . . .	11
2.4 Comparison of the averaged macroscopic stress-strain response in shear of SERVE A and SERVE B of Figure 2.2. . . . .	11
3.1 Anisotropy in damage evolution corresponding to mutually perpen- dicular loading of RVE 1 in Figure 4.3(a) . . . . .	19
3.2 Area fraction of cracked inclusions $\rho$ as a function of the principal strain $e_1$ of RVE 1 in Figure 4.3(a) for an instantaneous change in loading strain rate from $0.75 \text{ s}^{-1}$ to $0.25 \text{ s}^{-1}$ . . . . .	22
3.3 Area fraction of cracked inclusions $\rho$ as a function of the principal strain $e_1$ of RVE 1 in Figure 4.3(a) for an instantaneous change in loading strain rate from $0.25 \text{ s}^{-1}$ to $0.75 \text{ s}^{-1}$ . . . . .	23
4.1 Yield stress in shear $Y_f$ for the SERVE A shown in Figure 2.2(c) . .	25

4.2	Evolution of anisotropy parameters F,G and H with plastic work for SERVE A shown in Figure 2.2(c) . . . . .	27
4.3	(a) RVE 1 with hardcore distribution, (b) RVE 2 with equal sized elliptical inclusions. . . . .	29
4.4	Area fraction of cracked inclusions from LE-VCFEM analysis of RVE 1 shown in Figure 4.3(a) at a strain rate of $0.1 \text{ s}^{-1}$ along with the fit of Equation (3.17) . . . . .	32
4.5	Evolution of parameter $e_0$ with the local strain rate $\dot{\epsilon}$ from micromechanics VCFEM results along with the functional fit . . . . .	32
4.6	Evolution of parameter $m$ with the local strain rate $\dot{\epsilon}$ from micromechanics VCFEM results along with the functional fit . . . . .	33
4.7	Area fraction of cracked inclusions for the $y$ direction constrained tension LE-VCFEM analysis of RVE 1 shown in Figure 4.3(a) at a strain rate of $0.1 \text{ s}^{-1}$ along with the fit of Equation (3.17) . . . . .	34
4.8	Void nucleation anisotropy parameter $A$ as a function of the angle of principal strain $\theta_p$ . . . . .	35
5.1	Hardening (stress-strain) curve for the aluminum matrix used for the micromechanics LE-VCFEM simulations of RVE 1 in Figure 4.3(a) .	38
5.2	Macroscopic stress-strain response of the HCPD model and the homogenized micromechanical solutions for RVE 1 in Figure 4.3(a) . .	39
5.3	Macroscopic stress-strain response of the HCPD model and the homogenized micromechanical solution for RVE 1 in Figure 4.3(a) for strain ratio $e_{xx} \neq 0 : e_{yy} = 0 : e_{xy} = 0$ . . . . .	40
5.4	Comparison of macroscopic HCPD model simulation with the LE-VCFEM simulation of RVE 1 of Figure 4.3(a) subject to instantaneous change of strain rate from $0.25 \text{ s}^{-1}$ to $0.75 \text{ s}^{-1}$ at 0.6% applied strain. . . . .	42

5.5	Comparison of macroscopic HCPD model simulation with the LE-VCFEM simulation of RVE 1 of Figure 4.3(a) subject to instantaneous change of strain rate from $0.75 \text{ s}^{-1}$ to $0.25 \text{ s}^{-1}$ at 0.6% applied strain. . . . .	42
5.6	Macroscopic stress-strain response of the HCPD model and the homogenized LE-VCFEM solutions for RVE 1 in Figure 4.3(a) subject to different strain ratios $e_{xx} : e_{yy} : e_{xy}$ . . . . .	43
5.7	Parameter $C$ for RVE 1 in Figure 4.3(a) along with the independently calibrated values of $C$ for different strain ratios $e_{xx} : e_{yy} = 0 : e_{xy} = 0$	44

# CHAPTER 1

## INTRODUCTION

Metals and alloys containing heterogeneities e.g. particulates, precipitates, intermetallics, or voids in the microstructure are widely used in automotive, aerospace among other engineering systems. Figure 1.1 shows the micrograph of a Al-Si-Mg hypoeutectic cast aluminum alloy (AS7GU) used in the automotive industry. The microstructure comprises of (i) age-hardened aluminum matrix, strengthened by Mg/Si and Si precipitates, and (ii) a dispersion of brittle silicon particulates in the matrix. These heterogeneities can have adverse effects on failure properties like fracture toughness and ductility, and hence the need for including the morphology and distribution of these inclusions in the numerical model. The spatial distribution of the silicon inclusions and their morphology depends on the casting procedure used, and especially on the rate of heat extraction [1]. The solidification process tends to push particulates into the regions between the evolving secondary dendrite arms. The silicon inclusions are pinned in location once the eutectic temperature is reached. The secondary dendrite arm spacing (SDAS) of the microstructure depends on this solidification procedure. Cast alloys with small SDAS can be modeled readily, while alloys with large SDAS need to be modeled using a unique two-stage homogenization technique detailed in [2]. Ductile failure happens through micromechanical mechanisms

like particle fragmentation, interface debonding and matrix failure. Failure initiates by particle cracking, after which voids grow near the crack tips and subsequently coalesce to cause failure in the matrix. The nucleation and growth of the cracks are sensitive to local morphological parameters and constitutive parameters as shown in [3]. Damage evolution in microstructures are also sensitive to the applied strain rate as discussed in [32]. It is computationally expensive, if not impossible to simulate the entire microstructure with explicit representation of the heterogeneities, which has led to the development of the macroscopic rate-dependent homogenization based continuum plasticity damaged model. This macroscopic model has been designed to incorporate the morphological characteristics of the underlying microstructure, while saving computational time by working in a homogenized macroscopic scale.

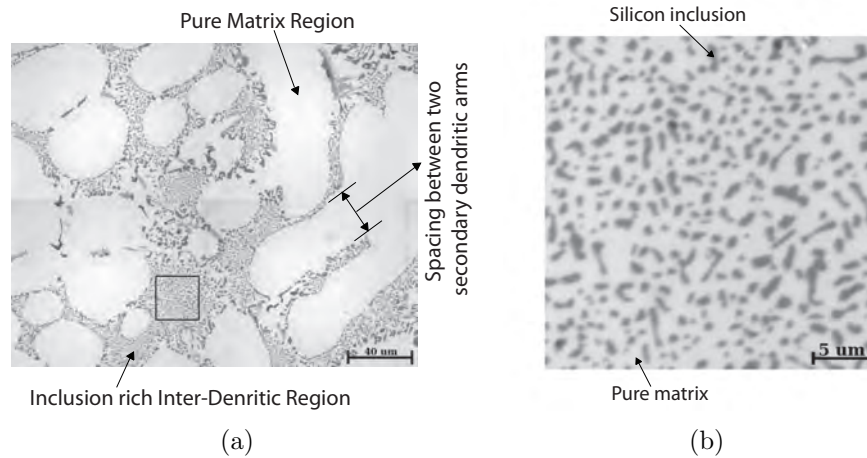


Figure 1.1: (a) Micrograph of a cast aluminum alloy AS7GU ( $120 \mu\text{m} \times 96 \mu\text{m}$ ), (b) blow-up of the designated region in (a) ( $28.4 \mu\text{m} \times 28.4 \mu\text{m}$ ).

## 1.1 Literature Survey

Various macroscopic constitutive models have been proposed to model heterogeneous material behavior and failure, based on morphological and phenomenological approaches. Most of the phenomenological models propose tensor or scalar damage variables whose evolution is governed by some evolution law, formulated from experimental observations. The general use of these phenomenological models is impeded by their lack of modeling the underlying physics and failure to explicitly account for the microstructure characteristics. On the other hand, models that incorporate morphological details solve boundary value problems of the representative volume element (RVE) to predict constitutive response at the macroscopic level. There are various analytical micromechanical models like those based on variational bounding methods e.g. [4, 5] and those based on effective medium approximations [6, 7]. These methods have limited capabilities for dealing with material nonlinearities, non-proportional load histories and complex morphologies. Multi-scale computational homogenization theories using asymptotic expansion [8, 9], where concurrent finite element analyses are executed at macro- and micro-scales with information transfer between them have been used for estimating averaged material properties of heterogeneous materials.

Ghosh and co-workers have combined the asymptotic homogenization method with the Voronoi cell finite element method (VCFEM), operating at the micro-scale for multi-scale analysis of deformation and damage in non-uniformly distributed microstructures in [10, 11, 12]. However, these approaches are computationally very expensive because of the detailed micromechanical analysis that needs to be performed at every integration point of macroscopic elements. To overcome the shortcomings of

simultaneous macro-micro modeling, [13] have developed the *homogenization based continuum plasticity-damage* or *HCPD* model for ductile materials containing heterogeneities that are undergoing ductile failure with evolving porosity. The HCPD model follows the Gurson-Tvergaard-Needleman or GTN models framework established in [14, 15, 16, 17] that account for void nucleation, growth and coalescence. GTN models where matrix anisotropy has been characterized by Hill's quadratic yield criterion have been proposed in [18, 19]. Studies in [20] have shown that the yield surface of porous materials with rigid inclusions retain the form of the GTN yield surface. This dissertation deals with the extension of the constitutive model proposed in [13] into a rate-dependent framework. A specific focus of this dissertation is the proposal of a new and novel damage evolution law, which is also rate-dependent. This model can be used effectively in the macroscopic simulation of ductile fracture in a multi-scale framework, owing to the extremely reduced computational time while retaining the morphological characteristics of the underlying microstructure.

## 1.2 Thesis Overview

The thesis is organized as follows. Chapter 2 introduces the computational tools required for the development of the rate-dependent HCPD model. Major parts of the rate-dependent HCPD model are described in Chapter 3. Chapter 4 describes the procedure for calibration of the model parameters. Numerical validation and examples are provided in Chapter 5 and Chapter 6 lists the scope for future work and conclusion.

## CHAPTER 2

### TOOLS NEEDED FOR DEVELOPING THE RATE-DEPENDENT HCPD MODEL

This chapter introduces the computational tools utilized in developing the rate-dependent homogenization based continuum plasticity damage model. Each of the sub-section explains briefly about a tool and references are provided for further understanding.

#### 2.1 Identification of the statistically equivalent RVE size

For the determination of the effective material properties of a microstructural domain, e.g. the inter-dendritic region of Figure 1.1(b), identifying the microstructural statistically equivalent RVE or SERVE is very important. A SERVE may be defined as the smallest volume element of the microstructure exhibiting the following characteristics [21, 22]:

- Effective constitutive material properties in the SERVE should be equivalent to properties of the entire microstructure, at least locally to within a prescribed tolerance.

- Distribution functions of parameters reflecting the local morphology, (local volume fraction, neighbor distance or radial distributions) in the SERVE should be similar to those for the overall microstructure within a prescribed tolerance.
- SERVE should be independent of the location in the local microstructure as well as of the applied loading direction.

Swaminathan et al. in [21, 22] have developed different techniques, like convergence of elastic stiffness tensor, two point correlation for anisotropy etc. for determination of SERVE size both without and with microstructural damage. The marked correlation function, first introduced by Pyrz [23] was used in [13, 2] to establish the SERVE size for porous ductile materials with a dispersion of heterogeneities. The marked correlation function  $M(r)$  is a multivariate characteristic function of the microstructure that relates any state variable (eg. stresses, strains or their dependent functions) with the microstructural morphology and distribution. It is expressed as a ratio of the state variable dependent function  $h(r)$  and the pair distribution function  $g(r)$  as:

$$M(r) = \frac{h(r)}{g(r)} \quad (2.1)$$

where

$$h(r) = \frac{1}{2\pi r} \frac{dH(r)}{dr} \quad \text{and} \quad H(r) = \frac{1}{m^2} \frac{A}{N^2} \sum_{i=1}^N \sum_{k=1}^{k_i} m_i m_k(r) \quad (2.2)$$

Here  $m_i$  represents a mark associated with the  $i$ -th inclusion,  $r$  is a measure of the radial distance of influence,  $m_k(r)$  corresponds to the mark associated with the  $k$ -th inclusion at a radial distance  $r$  and  $m$  is the mean of all marks.  $N$  is the total number of inclusions within the area  $A$  of the microstructural domain being analyzed and  $k_i$  is the number of inclusions that have their center within a circle of radius  $r$  centered at the  $i$ -th inclusion. The mark can be any chosen variable field in the microstructure

that has relevance the problem being pursued. The definition of the pair distribution function  $g(r)$  in Equation (2.1) is given as

$$g(r) = \frac{1}{2\pi r} \frac{dK(r)}{dr} \quad \text{and} \quad K(r) = \frac{A}{N^2} \sum_{k=1}^N I_k(r) \quad (2.3)$$

The pair distribution function  $g(r)$  characterizes the occurrence intensity of inter-inclusion distances.  $I_k(r)$  is the number of inclusions excluding the one being considered that lie inside the circle of radius  $r$ . The definition of the second-order intensity function  $K(r)$  is given in [21]. A high value of  $M(r)$  indicates a strong correlation between entities in the microstructure. As discussed in [2, 13],  $M(r)$  provides a good estimate of the size of the SERVE, for a local microstructure. It stabilizes to near-unity values at a characteristic radius of convergence  $r_0$ . For  $r \geq r_0$ ,  $M(r) \approx 1$  and the local morphology ceases to have any significant influence on the state variables beyond this characteristic radial distance. The radius of convergence  $r_0$  provides a good estimate for the SERVE size.

As discussed in [2, 21], a combination of three geometric parameters are used to calculate the SERVE size of the microstructure. The mark  $m_i$  associated with each inclusion is defined as a weighted average of local area fraction (LAF), inverse near neighbor distance (IND) and the number of near neighbors (NN) of that inclusion:

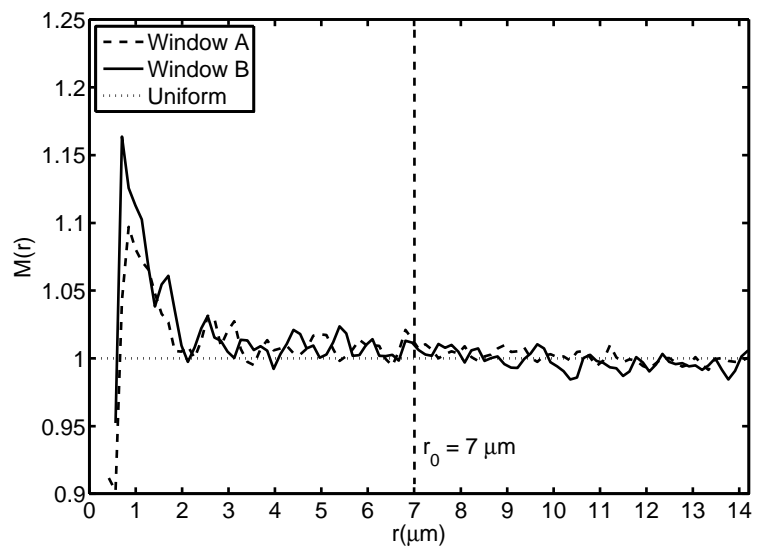
$$m_k = w_1 S_1^k + w_2 S_2^k + w_3 S_3^k \quad (2.4)$$

with

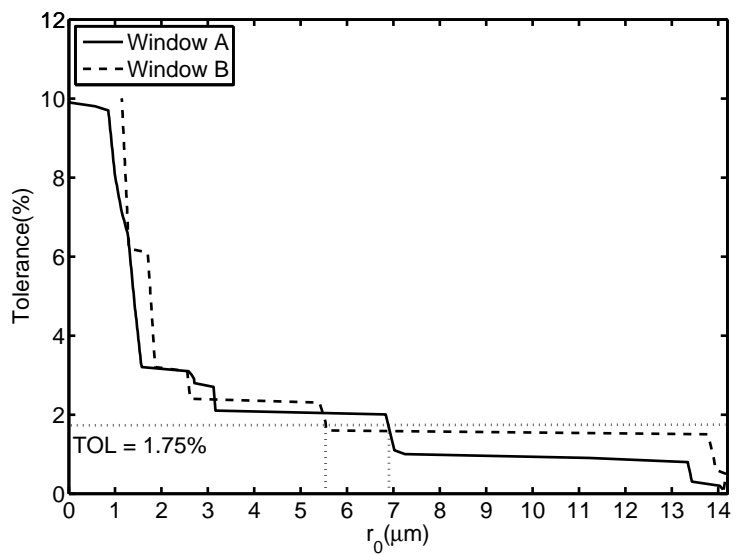
$$S_1^k = \frac{(LAF)^k}{\max_{1 \leq j \leq N} (LAF)^j} \quad ; \quad S_2^k = \frac{(IND)^k}{\max_{1 \leq j \leq N} (IND)^j} \quad ; \quad S_3^k = \frac{(NN)^k}{\max_{1 \leq j \leq N} (NN)^j}$$

where  $N$  is the total number of inclusions and  $(LAF)^k$ ,  $(IND)^k$ , and  $(NN)^k$  are the local area fraction, the inverse of the near-neighbor distance, and the number of near-neighbors of the  $k$ -th inclusion. Further details about calculating these quantities are given in [2]. From the micrograph shown in Figure 1.1(b), the marked correlation function in Equation (2.1) is calculated with the geometric mark of Equation (2.4). Weights  $w_1 = 1.0$ ,  $w_2 = 2.0$  and  $w_3 = 1.0$  are used, as suggested in [21].  $M(r)$  distributions are plotted in Figure 2.1(a), showing the convergence to  $M(r) = 1$  with varying  $r$ . In order to choose the tightest possible tolerance, the size of the SERVE corresponding to different acceptable tolerances for convergence are evaluated in Figure 2.1(b). This analysis suggests  $r_0 \approx 7 \mu\text{m}$  based on the highest value for the two regions using a tolerance of 1.75%. Correspondingly, the SERVE size is estimated as  $L_{SERVE} = 2 \times r_0 = 14 \mu\text{m}$ .

In order to verify the location independence of the 14  $\mu\text{m}$  SERVE, two different SERVE's are chosen from the microstructure and their respective homogenized responses are compared in rate-independent shear loading. The SERVE boundaries are created by periodically repeating the position of inclusions in the  $x$  and  $y$  directions, followed by drichlet tessellation [24, 25, 26]. The resulting SERVE's with the Voronoi cell mesh are shown in Figure 2.2. Their respective area fraction of inclusions are 18.31% and 18.45%, which are very close to the overall area fraction of the microstructural region of Figure 1.1(b) (18.62%). The elastic properties considered for micromechanical simulations are  $E_{Si} = 165 \text{ GPa}$  and  $\nu_{Si} = 0.27$  for the inclusions and  $E_{Al} = 70 \text{ GPa}$  and  $\nu_{Al} = 0.32$  for the matrix. The plastic hardening curve of the matrix is shown in Figure 2.3 and the initial yield stress is  $\sigma_y = 88.5 \text{ MPa}$ . The



(a)



(b)

Figure 2.1: (a) Marked correlation function for two different windows A and B using the mark of Equation (2.4), (b) radius of convergence  $r_0$  based on the results of (a) as a function of the chosen tolerance.

averaged macroscopic stress-strain response in shear for the two SERVE's of Figure 2.2 is shown in Figure 2.4. The results for the two SERVE's match very well with each other. This justifies the choice of  $L_{SERVE} = 14 \mu\text{m}$  and also proves the location independence.

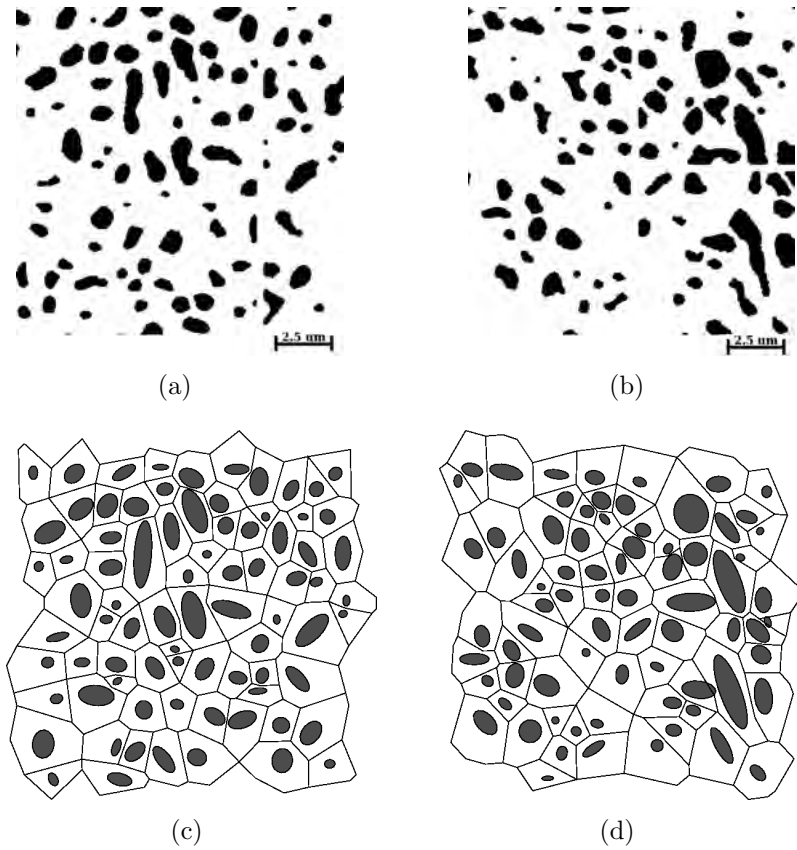


Figure 2.2: (a) Micrograph of the microstructural domain of SERVE A, (b) micrograph of the microstructural domain of SERVE B, (c) SERVE A with periodic boundary, (d) SERVE B with periodic boundary.

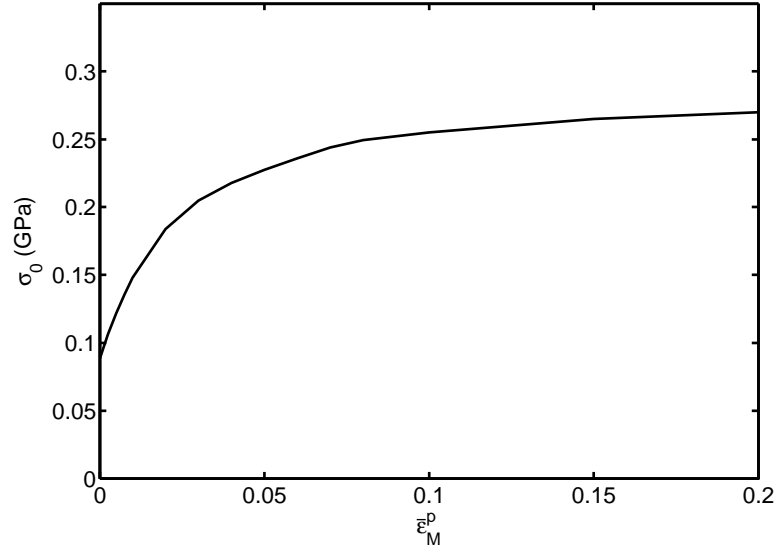


Figure 2.3: Hardening (stress-strain) curve for the aluminum matrix used for comparison of macroscopic behavior in shear for SERVE A and SERVE B of Figure 2.2.

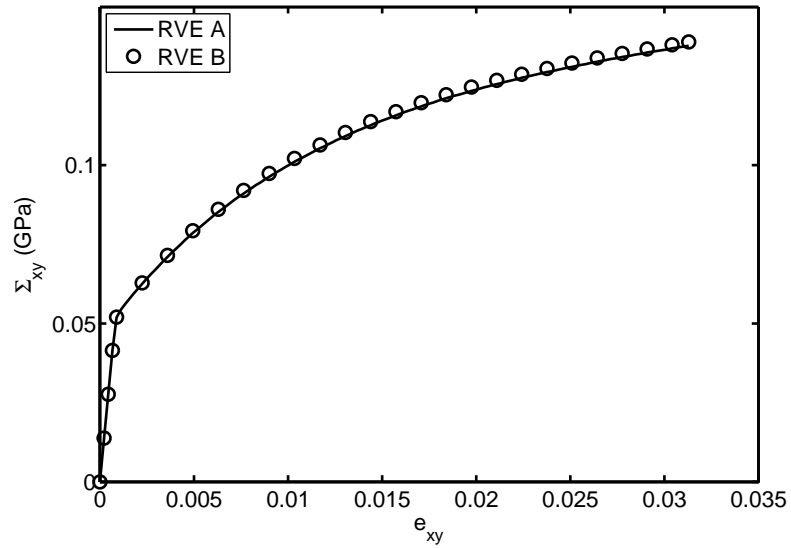


Figure 2.4: Comparison of the averaged macroscopic stress-strain response in shear of SERVE A and SERVE B of Figure 2.2.

## 2.2 Homogenization of micromechanical variables in RVE analysis

Development of the rate-dependent HCPD model requires evaluation of material properties from homogenized stresses, strains and other state variables. The asymptotic expansion homogenization method has been developed in [8, 9] for homogenized constitutive models of heterogeneous materials. Ghosh et al. have introduced a novel implementation of the asymptotic homogenization method, coupling macroscopic analysis with micromechanical VCFEM analysis of the RVE, in [11, 12, 27, 28]. The asymptotic homogenization method is implemented in conjunction with micromechanical elastic-plastic damage analysis of the RVE  $Y$  by LE-VCFEM in [13], which is used in the present work. The incremental form of the homogenized macroscopic stress-strain relation  $\Delta\Sigma_{ij} = E_{ijkl}^H \Delta\bar{e}_{kl}$  is obtained by volume averaging stresses and strains over the RVE. For this, the LE-VCFEM generated microstructural variables are integrated as:

$$\begin{aligned}\Sigma_{ij} &= \frac{1}{Y} \int_Y \sigma_{ij}^\epsilon(y) dY \\ \bar{e}_{ij} &= \frac{1}{Y} \int_Y e_{ij}^\epsilon(y) dY\end{aligned}\tag{2.5}$$

where  $\sigma_{ij}^\epsilon$  and  $e_{ij}^\epsilon$  are the microscopic stress and strain tensor in the RVE.  $E_{ijkl}^H$  is the homogenized elastic-plastic tangent modulus in the macroscopic constitutive law. Additionally, the rates of macroscopic void volume fraction ( $f$ ) and plastic work ( $W_p$ ) are defined as

$$\dot{f} = \frac{1}{Y} \int_Y \dot{f}^\epsilon dY, \quad \dot{W}_p = \frac{1}{Y} \int_Y \sigma_{ij}^\epsilon \dot{e}_{ij}^{\epsilon p} dY\tag{2.6}$$

where  $\mathbf{e}^{\epsilon p}$  is the microscopic plastic strain tensor in the RVE. For plane strain problems, components of  $E_{ijkl}^H$  can be obtained by averaging stress increments in response

to three separate imposed unit macroscopic strains increments  $\Delta\bar{\epsilon}_{ij}$  and solving the boundary value problems for the RVE. Details of this process can be found in [11, 12, 27, 28].

### **2.3 Locally enhanced voronoi cell finite element model (LE-VCFEM)**

Solutions of the micromechanical boundary value problem in the SERVE are necessary to provide data for the asymptotic expansion homogenization described in Chapter 2.2. The Voronoi locally enhanced cell finite element method or LE-VCFEM, developed by Ghosh et al. [29, 30, 31, 32] readily provides an accurate and extremely efficient means for micromechanical analysis of deformation and failure in arbitrary heterogeneous microstructures. Morphological non-uniformities in the heterogeneities, like orientations, shapes, and sizes of inclusions are conveniently modeled by this method. In [32, 33] the VCFEM model has been extended for rate-dependent elastic-viscoplastic porous ductile material. Micromechanical analysis in the present paper uses the VCFEM model in [32, 33]. The inclusions are linear elastic, while the matrix constitutive relations follow the over-stress viscoplastic model model of Perzyna [34].

## CHAPTER 3

### RATE-DEPENDENT HOMOGENIZATION BASED CONTINUUM PLASTICITY DAMAGE MODEL

The rate-dependent homogenization based continuum plasticity damage model framework is based on the anisotropic Gurson-Tvergaard-Needleman model following the developments of [18, 19], with the rate-dependency modeled through an over-stress model as described in [32, 2]. The tools described in Chapter 2, namely asymptotic expansion homogenization (AEH), LE-VPFEM are used in the development of this model.

In this constitutive model, the total strain rate is assumed to be additively decomposed into an elastic and viscoplastic part as:

$$\dot{\mathbf{e}} = \dot{\mathbf{e}}^e + \dot{\mathbf{e}}^p \quad (3.1)$$

For small elastic strains, the rate of Cauchy stress  $\dot{\Sigma}$  is related to the elastic part of the strain rate tensor as:

$$\dot{\Sigma} = \mathbf{C}^e : \dot{\mathbf{e}}^e \quad (3.2)$$

where  $\mathbf{C}^e$  is a fourth order anisotropic elasticity tensor. The anisotropic yield function for the porous ductile materials containing inclusions is expressed in terms of the

deviatoric and hydrostatic components of stress tensor as:

$$\phi = \frac{\Sigma_{eq}^2}{Y_f^2(W_p)} + 2Q_1 f \cosh\left(\frac{3Q_2}{2} \frac{\Sigma^{hyd}}{Y_f(W_p)}\right) - 1 - (Q_1 f)^2 \geq 0 \quad (3.3)$$

where  $\Sigma_{eq}$  and  $\Sigma^{hyd}$  are the homogenized equivalent and hydrostatic stress respectively and  $f$  is the macroscopic void volume fraction. The homogenized equivalent stress is defined in the Equation (3.11) and the hydrostatic stress is  $\Sigma^{hyd} = \frac{\Sigma_1 + \Sigma_2 + \Sigma_3}{3}$ .  $Y_f$  is the homogenized yield stress of the heterogenous material without any voids, expressed as a function of the inelastic work  $W_p$ . The effect of strain work-hardening is incorporated by this yield strength  $Y_f(W_p)$ , whose functional form is determined from the homogenization process. The parameters  $Q_1$  and  $Q_2$  govern the void evolution in the macroscopic model and are calibrated from the homogenization of the response of the RVE. In case of rate-independence, the Equation (3.3) becomes  $\phi = 0$ . The rate-dependency is modeled with the over-stress viscoplastic model developed in [34]. In this model, the viscoplastic strain rate and the rates of plastic work and void volume fraction are expressed as:

$$\dot{\mathbf{e}}^P = \dot{\Lambda} \mathbf{N}, \mathbf{N} = \frac{\partial \phi^*}{\partial \Sigma} \quad (3.4)$$

where  $\phi^*$  is given by Equation 3.9.

$$\dot{f} = \dot{f}_{growth} + \dot{f}_{nucleation} \quad (3.5)$$

$$\dot{W}_p = \Sigma : \dot{\mathbf{e}}^P \quad (3.6)$$

The homogenized void growth law is the same as the one used in [13] and is given by  $\dot{f}_{growth} = (1 - f)\dot{e}_{kk}^P$ , which results from plastic incompressibility of the underlying matrix without voids. The void nucleation law,  $\dot{f}_{nucleation}$  is one of the highlights of this dissertation and is explained in detail in Chapter 3.2. In Equations (3.4) , (3.5)

and (3.6) ,  $\dot{\Lambda}$  is the macroscopic viscoplastic multiplier.  $\dot{\Lambda}$  is obtained by assuming that the Hill-Mandel micro-macro energy condition [35] governs the homogenization conditions for the porous ductile materials. The rate of dissipative energy in the porous matrix material with incusions can be expressed as:

$$\Sigma : \dot{\mathbf{e}}^{\mathbf{P}} = (1 - f)\sigma^*\dot{\epsilon}^p = \dot{\lambda}(1 - f)\sigma : \epsilon^{\mathbf{P}} \quad (3.7)$$

where  $\sigma^*$  is the effective stress and  $\dot{\epsilon}^p$  is the effective plastic strain rate in the matrix with incusions in the absence of voids.  $\sigma$  and  $\epsilon^p$  are the stress and strain tensors in the matrix with incusions in the absence of voids. The viscoplastic multiplier in the matrix with incusions in the absence of voids is  $\dot{\lambda} = \Gamma_0\Phi(F)$ . Here,  $\Gamma_0$  is the temperature dependent viscosity co-effecient. In [34] a power law expression, i.e.  $\Phi(F) = \langle F \rangle^P$  has been discussed to adequately represent the behavior of most metals.  $\langle \ \rangle$  is the MacCauley operator corresponding to the positive sign of the argument. The over-stress  $F$  is a measure of the excess stress over the rate-independent local yield strength  $Y_f$  (an internal state variable), i.e.

$$F = \Sigma^* - Y_f(W_p) \quad (3.8)$$

where  $\Sigma^* = \sigma^*$  and can be obtained by setting

$$\phi^* = \frac{\Sigma_{eq}^2}{(\Sigma^*)^2} + 2Q_1f \cosh\left(\frac{3Q_2}{2} \frac{\Sigma^{hyd}}{\Sigma^*}\right) - 1 - (Q_1f)^2 = 0 \quad (3.9)$$

From the constitutive model discussed in [2] for non-porous matrix with incusions, the effective plastic strain rate in matrix with incusions in the absence of voids is derived as  $\dot{\epsilon}^p = \dot{\lambda}$ . From Equation (3.7) and (3.4) we can obtain the expression for the macroscopic viscoplastic multiplier,  $\dot{\Lambda}$  as:

$$\dot{\Lambda} = \frac{(1 - f)\Sigma^*}{\Sigma : \mathbf{N}} \Gamma_0\Phi(F) \quad (3.10)$$

The set of Equations (3.1)-(3.6), (3.8)-(3.10) form the constitutive model for the rate-dependent macroscopic simulation of porous ductile material with inclusions, i.e. the rate-dependent HCPD model. The entire constitutive model described above is expressed in an evolving principal material co-ordinate system or PDCS, which takes care of the evolving anisotropy. This unique feature of the model is explained below.

### 3.1 Evolving Anisotropy

As discussed in [13, 2], initial macroscopic material anisotropy is due to the presence of heterogeneities, e.g. brittle inclusions, in the microstructure. Furthermore, this anisotropy evolves with deformation due to nonuniform and constrained plastic flow in micro-channels between heterogeneities. The equivalent stress  $\Sigma_{eq}$  in the expressions (3.3) and (3.9) is designed to accommodate both initial and evolving anisotropy. For plane strain problems, it is expressed using the 3D anisotropic yield function in Hill [36] as:

$$\Sigma_{eq}^2 = F(\Sigma_{22} - \Sigma_{33})^2 + G(\Sigma_{33} - \Sigma_{11})^2 + H(\Sigma_{11} - \Sigma_{22})^2 + C\Sigma_{12}^2 \quad (3.11)$$

The stress components (and other tensor variables) in the constitutive model are represented in the principal axes of material anisotropy. The material is assumed to remain orthotropic in this system throughout the deformation process. The use of this material coordinate system has been shown in [13] to capture the effects of non-proportional load and deformation histories with very good accuracy. The angle  $\beta$ , delineating the principal axes of anisotropy for plane strain analysis, is determined in every increment from the condition that the transformed tangent modulus  $(E_{ijkl}^{\tan})'$  in this system remains orthotropic. This condition renders the terms coupling normal

and shear components of the tangent modulus to be equal to zero, i.e.

$$(E_{1112}^{\text{tan}})' = (E_{2212}^{\text{tan}})' = (E_{3312}^{\text{tan}})' = 0, \quad (3.12)$$

where  $(E_{ijkl}^{\text{tan}})' = Q_{im}Q_{jn}Q_{kp}Q_{lq}E_{mnpq}^{\text{tan}}$  and

$$[\mathbf{Q}] = \begin{bmatrix} \cos\beta & \sin\beta & 0 \\ -\sin\beta & \cos\beta & 0 \\ 0 & 0 & 1 \end{bmatrix}$$

Anisotropy parameters  $F$ ,  $G$ ,  $H$ , and  $C$  in Equation (3.11) are calibrated with respect to this principal coordinate system from homogenization. These parameters evolve due to the constrained plastic flow resulting from the presence of heterogeneities.

### 3.2 Rate-Dependent Void Nucleation Criterion

Ductile failure initiates with inclusion fragmentation and is followed by void evolution in the matrix. This microstructural mechanism manifests in the macroscopic rate-dependent HCPD model as void nucleation. The void nucleation model being developed in this dissertation is based on the work done by Ghosh et al. [13], where a strain-based rate-independent nucleation law is proposed and is proved to offer excellent agreement with the micromechanics VCFEM results. As discussed in [3, 32], the morphology and distribution of inclusions is exceedingly significant in governing the damage propagation in a porous ductile material with heterogeneities. Damage evolution is highly anisotropic as shown in Figure 3.1 and the void nucleation model proposed in this dissertation allows for the representation of this anisotropy with ease. In addition to the morphological characteristics, the loading rate also plays a significant role in the damage evolution in the microstructure. Paquet et al. [32, 33] have conducted a sensitivity study of the ductile fracture with respect to the loading rates and have concluded that the applied strain rates play an important role

on the ductile fracture of rate-sensitive heterogenous materials. As the strain rate increases, the stress in the inclusions are much higher than for lower strain rates, which results in the incusions cracking at a much lower strain. In addition to this, the matrix phase undergoes lower plastic deformation at higher strain rates, therefore reducing void growth and localization of damage near cracked inclusions. Strain to failure is thus determined by the competition between the two effects. This effect of rate-dependency is also included in the proposed void nucleation model.

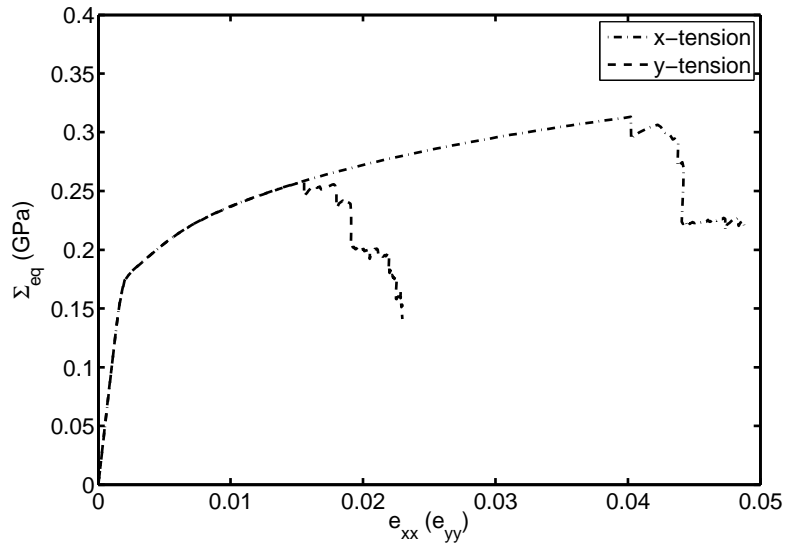


Figure 3.1: Anisotropy in damage evolution corresponding to mutually perpendicular loading of RVE 1 in Figure 4.3(a)

As in [13], the void nucleation model is based on the Weibull statistics-based probability of fracture  $\bar{P}_{fr}$ , which is parallel to the probability governing the cracking of inclusions in the microstructure as detailed in [13, 32]. The probability function

$\bar{P}_{fr}$  is written in terms of local strains as:

$$\bar{P}_{fr}(v, \hat{e}) = 1 - \exp \left[ -\frac{v}{v_0} \left( \frac{\hat{e}}{e_0} \right)^m \right] \quad (3.13)$$

where  $e_0$  and  $m$  are the Weibull parameters, which are functions of local strain rate  $\dot{\hat{e}}$ .  $\hat{e}$  is an effective strain measure expressed as:

$$\hat{e} = \langle Ae_1 + Be_2 + Ce_3 \rangle \quad (3.14)$$

where  $e_1, e_2$  and  $e_3$  are the local principal strains and  $\langle \ \rangle$  is the MacCauley operator corresponding to the positive sign of the argument.  $A, B$  and  $C$  are parameters that are calibrated from micromechanics VCFEM analysis of the RVE. The co-efficients  $A, B$  and  $C$  are functions of the angle of principal strain  $\theta_p$  and provide an efficient method for modeling the damage anisotropy emerging from morphology and distribution of inclusions in the microstructure. A new state variable, area fraction of cracked particles  $\rho$  is introduced to acomodate instantaneous variations in local strain rates. The area fraction of cracked inclusions for constant strain rate deformation  $\rho_c(\hat{e})$  is expressed in terms of the probability density function of the inclusion size  $p(v)$  and the probability of fracture  $\bar{P}_{fr}(v, \hat{e})$  as:

$$\rho_c(\hat{e}) = \int_0^\infty \frac{v}{v_0} p(v) \bar{P}_{fr}(v, \hat{e}) dv \quad (3.15)$$

If a discrete distribution of inclusions in a limited size RVE is to be considered, The probability density function  $p(v)$  can be written as

$$p(v) = \sum_{i=1}^N \delta(v - v_i) p(v_i) \quad (3.16)$$

where  $\delta()$  is the dirac delta function and  $N$  is the number of bins in the probability density function  $p(v)$ . Using Equation (3.16) in (3.15) gives:

$$\rho_c(\hat{e}) = \int_0^\infty \frac{v}{v_0} \left[ \sum_{i=1}^N \delta(v - v_i) p(v_i) \right] \bar{P}_{fr}(v, \hat{e}) dv$$

$$\rho_c(\hat{e}) = \sum_{i=1}^N \int_0^{\infty} \frac{v}{v_0} [\delta(v - v_i)p(v_i)] \bar{P}_{fr}(v, \hat{e}) dv$$

and can be simplified to

$$\begin{aligned} \rho_c(\hat{e}) &= \sum_{i=1}^N \frac{v_i}{v_0} p(v_i) \bar{P}_{fr}(v, \hat{e}) \\ \rho_c(\hat{e}) &= \sum_{i=1}^N \frac{v_i}{v_0} p(v_i) \left( 1 - \exp \left[ -\frac{v_i}{v_0} \left( \frac{\hat{e}}{e_o} \right)^m \right] \right) \end{aligned} \quad (3.17)$$

where  $p(v_i)$  is the probability of finding a inclusion of size  $v_i$ . If all the particles have the same size, i.e.  $p(v) = 1$ , the area fraction of cracked inclusion can be derived from Equation (3.17) as

$$\rho_c(\hat{e}) = 1 - \exp \left[ -\left( \frac{\hat{e}}{e_o} \right)^m \right] \quad (3.18)$$

The evolution of the state variable, area fraction of cracked particles  $\rho$  is governed by the equation

$$\dot{\rho} = \frac{d\rho_c(\hat{e})}{d\hat{e}} \dot{\hat{e}} \tilde{k}^* \quad (3.19)$$

Finally, the void nucleation for the rate-dependent HCPD model is given as

$$\dot{f}_{nucleation} = V_p \frac{d\rho_c(\hat{e})}{d\hat{e}} \dot{\hat{e}} \tilde{k}^* \quad (3.20)$$

where

$$\tilde{k} = \frac{1 - \rho}{1 - \rho_c(\hat{e})}, \quad \tilde{k}^* = \begin{cases} \tilde{k} & \text{if } \tilde{k} \geq 1 \\ 0 & \text{if } \tilde{k} < 1 \end{cases} \quad (3.21)$$

where  $\tilde{k}^*$  is a factor that takes care of the instantaneous change in strain rates. When there is an increase in local strain rate, the stress in the particles of the underlying microstructure increases and more particles start cracking. In order to incorporate this effect, the factor  $\tilde{k}$  is included in the void nucleation law to increase the nucleation of voids and bring it up to the actual value, as shown in Figure 3.2. When the local strain rate decreases, all the particles that will crack eventually have already cracked

(because of the higher stress in higher strain rates) and therefore no nucleation is necessary till the appropriate value is reached, as shown in Figure 3.3. The value  $\rho_c(\hat{e})$  in the denominator of Equation (3.21) is the area fraction of cracked particles at constant strain rate and is obtained from Equation (3.17) or (3.18). The parameter  $V_p$  in Equation (3.20) is calibrated from the volume fraction of cracked inclusions at given strain. The calibration procedure for the parameters  $e_0$ ,  $m$ ,  $V_p$ ,  $A$ ,  $B$  and  $C$  is detailed in Section 4.5.

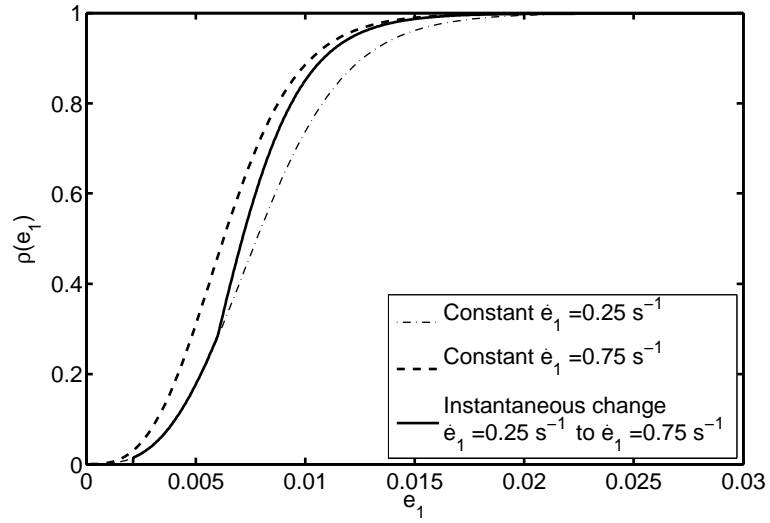


Figure 3.2: Area fraction of cracked inclusions  $\rho$  as a function of the principal strain  $e_1$  of RVE 1 in Figure 4.3(a) for an instantaneous change in loading strain rate from  $0.75 \text{ s}^{-1}$  to  $0.25 \text{ s}^{-1}$

### 3.3 Numerical implementation of the rate-dependent HCPD model

The numerical implementation of the macroscopic rate-dependent HCPD model follows the return mapping algorithm for rate-dependent plasticity developed in [37].

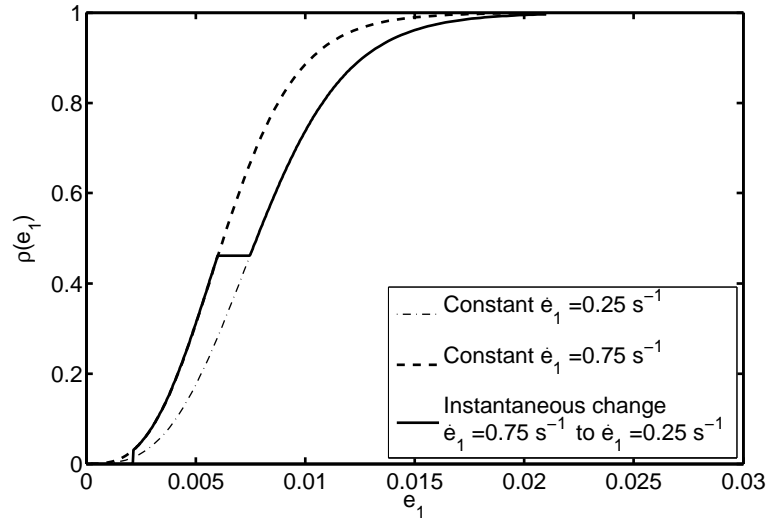


Figure 3.3: Area fraction of cracked inclusions  $\rho$  as a function of the principal strain  $e_1$  of RVE 1 in Figure 4.3(a) for an instantaneous change in loading strain rate from  $0.25 \text{ s}^{-1}$  to  $0.75 \text{ s}^{-1}$

The return mapping algorithm consists of an initial elastic predictor step, where the elastic response is assumed and the stresses are predicted. This is followed by the plastic corrector step which returns the stress to the updated yield surface. The numerical stress update algorithm is programmed in fortran and is used with *MSC Marc* through the *Uvscpl()* subroutine.

## CHAPTER 4

### CALIBRATION OF RATE-DEPENDENT HCPD MODEL PARAMETERS

The rate-dependent HCPD model parameters are calibrated from homogenized quantities such as macroscopic strain  $\mathbf{e}$ , plastic strain  $\mathbf{e}^P$ , stress  $\Sigma$  and plastic work  $W_p$  obtained from asymptotic expansion homogenization (AEH) of micromechanical variables from LE-VCFEM simulations. The parameters are calibrated in the material principal coordinate system following the procedure outlined for rate-independent materials in [13]. These are discussed next. The calibration procedure for the parameters of the void nucleation model is described in 4.5

#### 4.1 $Y_f(W_p)$ and $C$ in Equations (3.3, 3.11)

The flow stress in shear,  $Y_f(W_p)$  describes the hardening behavior of the homogenized material. In order to calibrate the evolution of  $Y_f(W_p)$ , a rate-independent LE-VCFEM based micromechanical RVE analysis is conducted for shear deformation, with  $e_{xx} = e_{yy} = 0$ ,  $e_{xy} \neq 0$ . The matrix material is assumed to be void free and no inclusion fragmentation is allowed. Micromechanical analysis is followed by homogenization, in which the macroscopic plastic work, stresses and strains are evaluated from the microstructural variables using equations (2.5) and (2.6). For pure

shear loading, the resulting macroscopic tensor is of the form  $\Sigma_{xx} = \Sigma_{yy} = \Sigma_{zz} = 0$  and  $\Sigma_{xy} \neq 0$ . From the Equations (3.3) and (3.11), the yield stress is calculated as

$$Y_f(W_p) = \sqrt{3}\Sigma_{xy} \quad (4.1)$$

where the parameter  $C$  in equation (3.11) is set to 3. The yield stress  $Y_f$  is plotted as a function of  $W_p$  in figure 4.1.

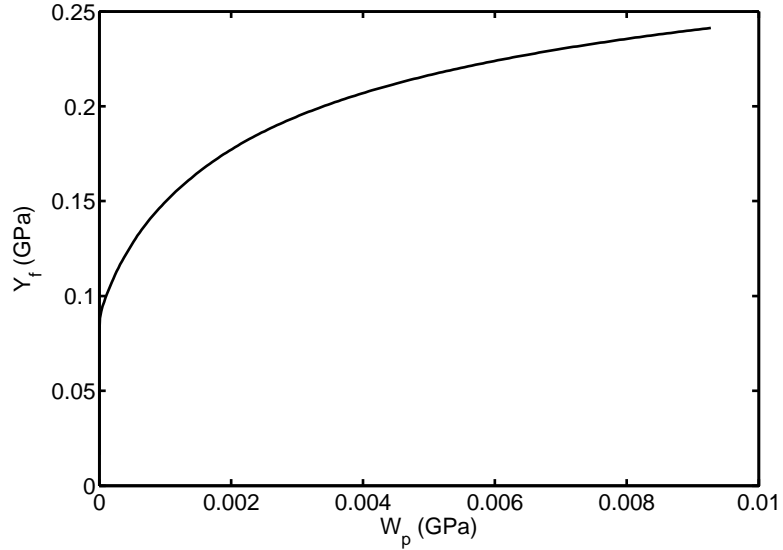


Figure 4.1: Yield stress in shear  $Y_f$  for the SERVE A shown in Figure 2.2(c)

## 4.2 Parameters $F, G$ and $H$ in equation (3.11)

For a given RVE, like the one shown in Figure 2.2(c), micromechanical LE-VCFEM simulations are performed for  $N$  different loading conditions, followed by homogenization. As with the calibration of  $Y_f$ , the simulations are rate-independent and no void evolution or inclusion cracking is allowed. Loading conditions are prescribed with different macroscopic strain ratios  $e_{xx} : e_{yy} : e_{xy}$ . A total of 18 different

loading conditions are used to calibrate the anisotropy parameters. At the end of each strain increment, the tangent stiffness  $E_{ijkl}^{\text{tan}}$  is evaluated and subsequently the material principal co-ordinate system is determined from Equation (3.12). Macroscopic stress tensor  $\Sigma$  and plastic work  $W_p$  are computed in the principal coordinate system using equations (2.5) for each load step. For a given value of plastic work  $W_p$ , the  $Y_f(W_p)$  is obtained from the evolution curve such as Figure 4.1. This is done for all the load histories. The plastic work dependent anisotropy parameters  $F(W_p)$ ,  $G(W_p)$ ,  $H(W_p)$  are then evaluated minimizing the least square residual of the rate-independent form of the Equation (3.11) as:

$$\min_{F,G,H} \sum_{i=1}^N [F(\Sigma_{22}^i - \Sigma_{33}^i)^2 + G(\Sigma_{33}^i - \Sigma_{11}^i)^2 + H(\Sigma_{11}^i - \Sigma_{22}^i)^2 + C(\Sigma_{12}^i)^2 - (Y_f^i)^2]^2 \quad (4.2)$$

For a given value of  $W_p$ ,  $N = 18$  points corresponding to the 18 different loadings are used. The parameters  $F$ ,  $G$ ,  $H$  are solved by an iterative algorithm with  $C = 3$ . The step is repeated for different values of  $W_p$  to obtain the evolution curves for  $F$ ,  $G$  and  $H$  as a function of  $W_p$ . The evolution of the anisotropy parameters  $F$ ,  $G$  and  $H$  for the RVE in Figure 2.2(c) is shown in Figure 4.2. While  $F$  and  $G$  reduce nonlinearly with  $W_p$ ,  $H$  increases with  $W_p$ . More study on the evolution of the anisotropy parameters in different RVE's has been done in [13]. This study shows that relatively isotropic microstructures have  $F \approx G$  and pronounced anisotropy results in  $F \neq G$ .

### 4.3 Viscoplastic parameters $\Gamma_0$ and $p$ in Equation (3.10)

The homogenized viscoplastic properties in the rate-dependent HCPD model are calibrated from a set of loading conditions combining  $M$  applied strain rates for  $N$  different imposed strain ratios  $e_{xx} : e_{yy} : e_{xy}$ . These simulations are done subject to zero initial void in the matrix, no void evolution and no particle cracking. At each

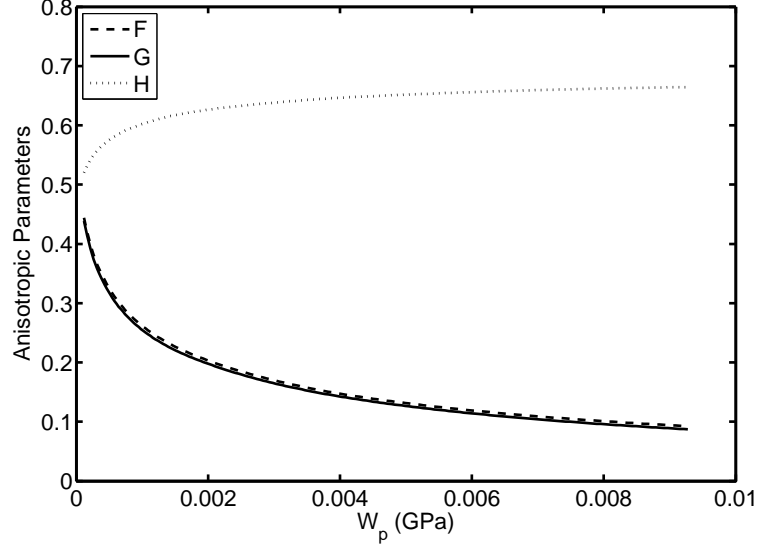


Figure 4.2: Evolution of anisotropy parameters F,G and H with plastic work for SERVE A shown in Figure 2.2(c)

increment, the principal coordinate system, the stress tensor  $\Sigma$  and the plastic work  $W_p$  are computed. The corresponding yield stress  $Y_f(W_p)$  and anisotropy coefficients  $F(W_p)$ ,  $G(W_p)$ ,  $H(W_p)$  are evaluated using the previously calibration results from Sections 4.1 and 4.2. The macroscopic viscoplastic properties are obtained by minimizing the square of the error between micromechanical analyses and macroscopic simulations using the rate-dependent HCPD model of Chapter 3, with the void nucleation and growth parts turned off. The error is defined as the Frobenius norm of the stress difference:

$$\min_{\gamma_0, P} \sum_{i=1}^N \sum_{j=1}^M \sum_{k=1}^{K_i} \|\Sigma_{\text{macro}}^{ijk} - \Sigma_{\text{micro}}^{ijk}\|_F^2 \quad (4.3)$$

where  $K_i$  is the number of applied increments in the simulations corresponding to the  $i$ -th load path. For the calibration of viscoplastic parameters, four different strain

rates in shear are applied, i.e.  $N = 3$  and  $M = 4$ . The applied strain rates are  $\dot{e}_{xy}^{(1)} = 0.01 \text{ s}^{-1}$ ,  $\dot{e}_{xy}^{(2)} = 0.03 \text{ s}^{-1}$ ,  $\dot{e}_{xy}^{(3)} = 0.06 \text{ s}^{-1}$  and  $\dot{e}_{xy}^{(4)} = 0.10 \text{ s}^{-1}$ .

#### 4.4 Parameters $Q_1$ and $Q_2$ in Equation (3.3)

The parameters,  $Q_1$  and  $Q_2$ , which govern the void evolution in the macroscopic rate-dependent HCPD model are calibrated from a set of micromechanical simulations, now with void evolution enabled. Homogenization is performed on these micromechanical simulations for evaluating the coefficients  $Q_1$  and  $Q_2$  in Equation (3.3). The following steps are undertaken for this objective.

1. An rate-independent LE-VCFEM simulation of the RVE is conducted with an applied macroscopic shear strain,  $e_{xx} = 0 : e_{yy} = 0 : e_{xy} \neq 0$  for plastic deformation and void evolution. The corresponding macroscopic stress tensor  $\Sigma$  and averaged void volume fraction  $f$  are evaluated and plotted as functions of the averaged matrix plastic work  $W_p$ . These averaged macroscopic quantities are obtained from homogenization as defined in Equation (2.6). Since the normal stresses  $\Sigma_{xx} = \Sigma_{yy} = \Sigma_{zz} = 0$  for this loading, and also the hydrostatic part of plastic strain  $e_{kk}^p = 0$ , the void volume fraction does not change, i.e.  $f = f_o$ . The parameter  $Q_1$  can be solved from the Equation (3.3) as:

$$Q_1 = \frac{1}{f_o} \left( 1 - \frac{\sqrt{3}\Sigma_{xy}}{Y_f} \right) \quad (4.4)$$

2. The same set of numerical simulations as in Section (4.2) is again performed for the microstructural RVE with non-zero, evolving void volume fractions. For a given value of plastic work  $W_p$ , the parameter  $Q_2$  is evaluated from known

values of  $F, G, H, Y_f$  and  $Q_1$  by solving the minimization problem

$$\min_{Q_2} \sum_{i=1}^N \left[ \frac{\Sigma_{eq}^2}{Y_f^2} + 2Q_1 f \cosh \left( \frac{3Q_2 \Sigma^{hyd}}{2 Y_f} \right) - 1 - (Q_1 f)^2 \right]^2 \quad (4.5)$$

where  $N = 18$  is the total number of loadings.

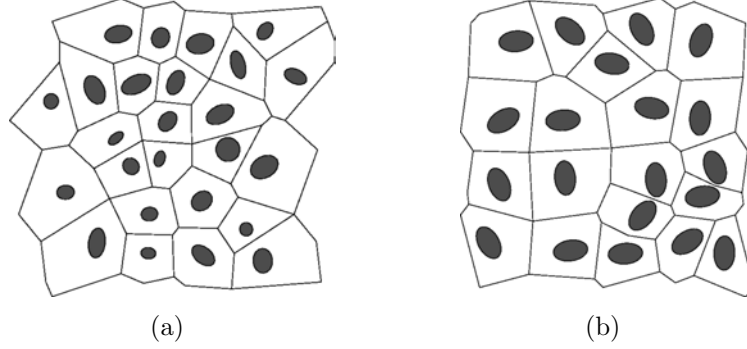


Figure 4.3: (a) RVE 1 with hardcore distribution, (b) RVE 2 with equal sized elliptical inclusions.

It has been shown by Ghosh et al. [13] that the calibrated values of  $Q_1$  and  $Q_2$  for the different RVEs exhibit only minimal dependence on plastic work and hence can be taken as constants. The mean and standard deviation of  $Q_1$  and  $Q_2$  for the two RVEs of Figures 4.3(a) and 4.3(b) are listed in Table 4.1. The standard deviations of  $Q_1$  and  $Q_2$  are very small compared to the mean values, and hence  $Q_1$  and  $Q_2$  for each RVE are taken as constants in the analyses, as concluded in [13]. The parameters  $Q_1$  and  $Q_2$  depend on the RVE they are calibrated from. The  $Q_1$  values are quite different from the value in the pure matrix material ( $q_1=1.5$ ). This difference is attributed to the effect of the inclusion volume fraction  $V_f$ . A sensitivity study has been conducted by Ghosh et al. [13] to relate the effect of the microstructure on the values of  $Q_1$

and  $Q_2$ . It has been identified that  $Q_1$  and  $Q_2$  have sole dependence on the volume fraction  $V_f$  of heterogeneities in the microstructure.

	Mean of $Q_1$	Standard Dev. of $Q_1$	Mean of $Q_2$	Standard Dev. of $Q_2$
RVE 1	1.70	0.0065	1.04	0.0179
RVE 2	1.77	0.0026	1.09	0.0064

Table 4.1: Mean and standard deviation of calibrated parameters  $Q_1$  and  $Q_2$  for different RVEs

## 4.5 Calibration of parameters in the void nucleation model

The calibration of parameters for the rate-dependent void nucleation criterion can be split into two distinct steps. The first step involves the calibration of the local strain-rate dependent parameters  $e_0$  and  $m$  in the Equations (3.17) and (3.18). The second step involves the calibration of parameters  $A, B$  and  $C$  in Equation (3.14), which take care of the anisotropy in damage evolution due to the morphology and distribution of the inclusions. These parameters  $A, B$  and  $C$  are functions of the angle of principal strain  $\theta_p$ . Rate-dependent LE-VCFEM simulations with void evolution and inclusion cracking along with the *rate-dependent HCPD* model analyses are conducted for calibrating all the required parameters.

### 4.5.1 $e_0$ and $m$ calibration

The parameters  $e_0$  and  $m$  in the Equations (3.17) and (3.18), defining the area fraction of cracked particles  $\rho(e)$  are functions of local strain rate. These two parameters govern the rate-dependency of damage evolution. In order to calibrate  $e_0$  and  $m$ , a total of  $K$  micromechanical LE-VCFEM simulations with strain rates spread

between the required range for the macroscopic HCPD model are performed. For the RVE 1 shown in Figure 4.3(a), a total of 10 LE-VCFEM simulations with strain rates between  $0.01 \text{ s}^{-1}$  and  $0.75 \text{ s}^{-1}$  were performed. All of the micromechanical simulations required for the calibration of  $e_0$  and  $m$  are performed under an applied macroscopic strain ratio  $e_{xx} \neq 0 : e_{yy} = 0 : e_{xy} = 0$ . For each of the  $K$  micromechanical simulations,  $e_0$  and  $m$  are calculated, so that a best fit is obtained between the Equation (3.17) or (3.18) and micromechanics results for the area fraction of cracked particles. Figure 4.4 shows the micromechanics result for the area fraction of cracked particles at an applied strain rate of  $0.1 \text{ s}^{-1}$  as a function of the principal strain  $e_1$  for the RVE 1 in Figure 4.3(a) along with the fitted curve of Equation (3.18) for the values  $e_0 = 0.009739$  and  $m = 3.11$ . For this applied strain ratio of  $e_{xx} \neq 0 : e_{yy} = 0 : e_{xy} = 0$ , the effective strain is,  $\hat{e} = Ae_1$  and the parameter  $A(\theta_p = 0^\circ) = 1$ .

Once the calibration has been completed for all the  $K$  applied strain rates, the functional forms for the parameters  $e_0$  and  $m$  can be obtained as a function of the local strain rate  $\dot{\hat{e}}$ . Figure 4.5 and 4.6 show the discrete calibrated values and the functional fit for the parameters  $e_0$  and  $m$  calibrated from the RVE 1 in Figure 4.3(a). It can be observed in the Figure 4.5 and 4.6 that there are two distinct mechanisms taking place due to the rate-dependency. At lower strain rates, along with particle cracking, voids start to nucleate near the tip of the cracked inclusions and subsequently coalesce to cause matrix failure in the microstructure. This results in damage localization and failure of the material. On the other hand, at higher strain rates, the matrix starts to behave more elastic and therefore the void nucleation in the matrix and growth is reduced and no localization of damage happens in the microstructure.

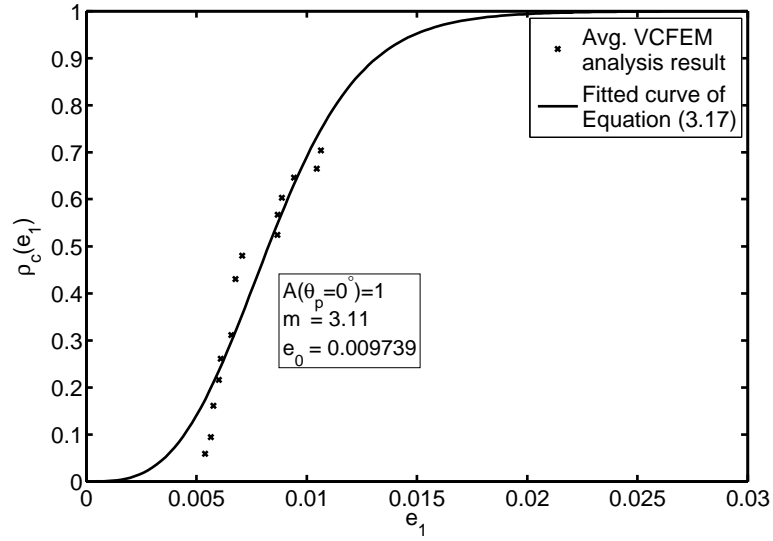


Figure 4.4: Area fraction of cracked inclusions from LE-VCFEM analysis of RVE 1 shown in Figure 4.3(a) at a strain rate of  $0.1 \text{ s}^{-1}$  along with the fit of Equation (3.17)

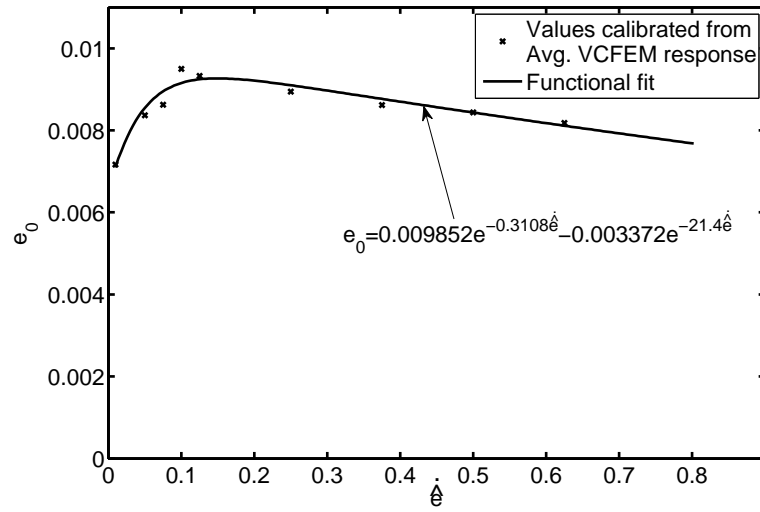


Figure 4.5: Evolution of parameter  $e_0$  with the local strain rate  $\dot{\epsilon}$  from micromechanics VCFEM results along with the functional fit

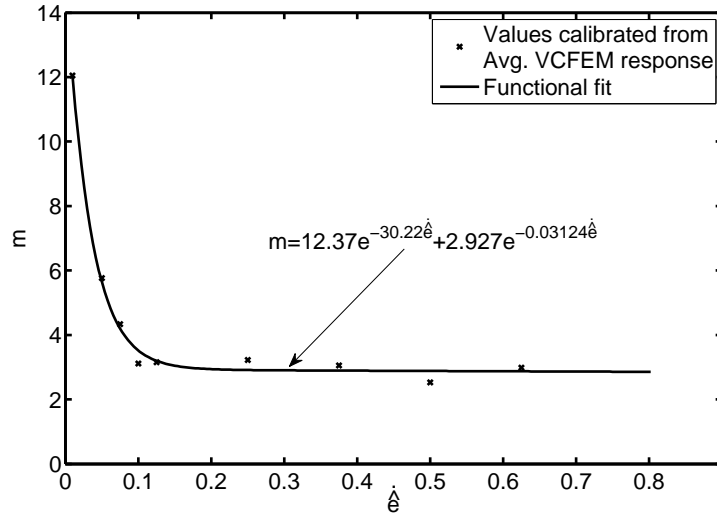


Figure 4.6: Evolution of parameter  $m$  with the local strain rate  $\dot{\epsilon}$  from micromechanics VCFEM results along with the functional fit

#### 4.5.2 A, B and C calibration

In order to calibrate the anisotropy parameters  $A$ ,  $B$  and  $C$ , a total of four LE-VCFEM simulations at any strain rate, chosen between the limits used in Section 4.5.1 are needed. The four simulations with different loading conditions are

1. Tension tests in the  $y$  directions, with zero transverse strains ( $e_{xx} = 0 : e_{yy} \neq 0 : e_{xy} = 0$ ),
2. Biaxial tension test ( $e_{xx} = e_{yy} \neq 0 : e_{xy} = 0$ ),
3. Two simulations with strain ratios ( $e_{xx} > 0 : e_{yy} < 0 : e_{xy} = 0$ ) and ( $e_{xx} < 0 : e_{yy} > 0 : e_{xy} = 0$ )

The anisotropy parameters  $A$ ,  $B$  and  $C$  have the functional form of an ellipse, and at any given angle of principal strain  $\theta_p$ , the value of  $A$ ,  $B$  or  $C$  is the radius of the

ellipse. In the Section 4.5.1, the radius of the ellipse describing the parameter  $A$  at  $\theta_p = 0^\circ$  is assumed to be 1. This value  $A(\theta_p = 0^\circ) = 1$  is one of the axes of the ellipse describing  $A$ . The other axis of the ellipse is obtained from the  $y$  direction constrained tension test (1). For the RVE 1 shown in Figure 4.3(a), the area fraction of fractured inclusion  $\rho$  is plotted as a function of the principal strain  $e_1$  in Figure 4.7. In this constrained  $y$  loading condition, value of  $A$  at  $\theta_p = 90^\circ$  is evaluated by fitting either Equation (3.17) or (3.18) with the micromechanics result shown in Figure 4.7. The value of  $e_0$  and  $m$  at the effective strain rate  $\dot{\epsilon}$  are obtained from the functional forms calibrated in the Section 4.5.1. Figure 4.8 shows the functional form of the parameter  $A$  as a function of the angle of principal strain  $\theta_p$ .

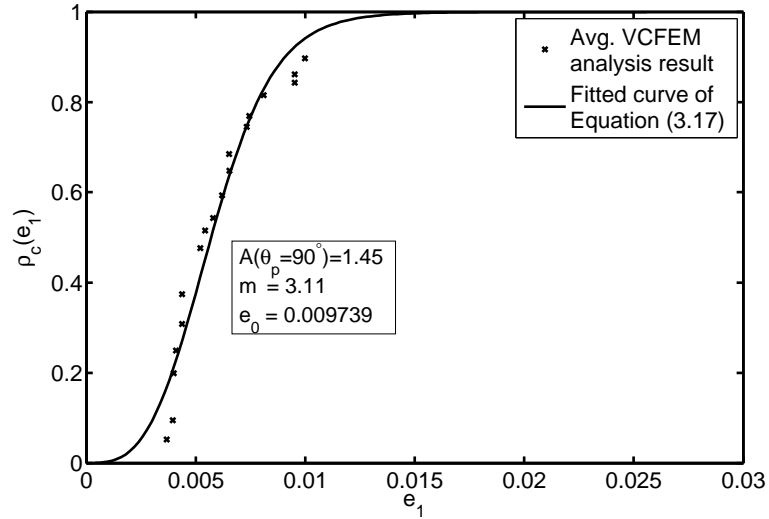


Figure 4.7: Area fraction of cracked inclusions for the  $y$  direction constrained tension LE-VCFEM analysis of RVE 1 shown in Figure 4.3(a) at a strain rate of  $0.1 \text{ s}^{-1}$  along with the fit of Equation (3.17)

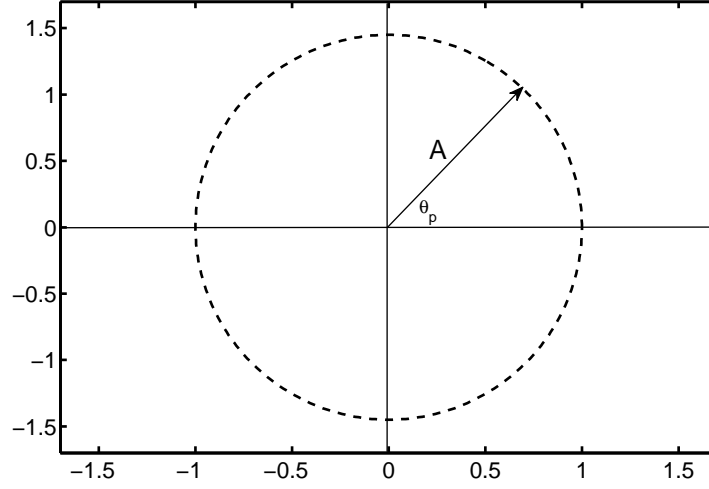


Figure 4.8: Void nucleation anisotropy parameter  $A$  as a function of the angle of principal strain  $\theta_p$

Similar to  $A$ , the major and minor axes of the ellipse describing the parameter  $B$  can be obtained from the biaxial tension test (2). Since for the biaxial tension test, the angle of principal strain  $\theta_p = 0^\circ$  or  $90^\circ$ , only one of the axes of the ellipse needs to be determined. If the angle of principal strain is taken as  $\theta_p = 0^\circ$ , then  $A(\theta_p) = 1$  and the effective strain is  $\hat{e} = Ae_1 + Be_2$ . Once again, either Equation (3.17) or (3.18) is fit with the micromechanics result for area fraction of cracked particles to evaluate the value of  $B$  at  $\theta_p = 0^\circ$ . The other axis of the  $B$ -ellipse can be obtained as

$$B(\theta_p = 90^\circ) = [A(\theta_p = 0^\circ) + B(\theta_p = 0^\circ) - A(\theta_p = 90^\circ)]$$

The other two loading conditions,  $(e_{xx} > 0 : e_{yy} < 0 : e_{xy} = 0)$  and  $(e_{xx} < 0 : e_{yy} > 0 : e_{xy} = 0)$  are used to calibrate the major and minor axis of the elliptical form of the

parameter  $C$ . The values of  $A, B$  and  $C$  for the RVEs 1 and 2 shown in the Figure 4.3 are given in the Table 4.2

	$A(\theta_p = 90^\circ)$	$B(\theta_p = 0^\circ)$	$B(\theta_p = 90^\circ)$	$C(\theta_p = 0^\circ)$	$C(\theta_p = 90^\circ)$
RVE 1	1.45	1.51	1.06	0.90	1.34
RVE 2	1.28	1.39	1.10	0.96	1.10

Table 4.2: Values of anisotropy parameters  $A, B$  and  $C$  at different angles of principal strain  $\theta_p$ . The value of  $A(\theta_p = 0^\circ) = 1$  for all RVEs

Subsequently the parameter  $V_p$ , which relates the volume fraction of cracked inclusions to the void nucleation rate in the rate-dependent HCPD model, is evaluated iteratively from several macroscopic numerical analyses, by minimizing the difference between the micromechanical and HCPD simulations :

$$\min_{V_p} \sum_{i=1}^N \sum_{j=1}^{M_i} \|\Sigma_{\text{HCPD}}^{ij} - \Sigma_{\text{micro}}^{ij}\|_F^2 \quad (4.6)$$

where  $N$  is the total number of simulations performed for the calibration of  $V_p$  and  $M_i$  is the number of increments in the  $i$ th micromechanical simulation.

## CHAPTER 5

### NUMERICAL EXAMPLES WITH THE RATE-DEPENDENT HCPD MODEL

The rate-dependent HCPD model is validated by comparing the results of the macroscopic finite element simulations with those obtained from the homogenization of the micromechanics LE-VCFEM results. An extensive validation of rate-independent HCPD model has been performed in [13], demonstrating the capability of the model for various proportional and non-proportional loading conditions. Since this rate-dependent HCPD model is an extension of the model proposed in [13], only the rate-effects and the novel rate-dependent void-nucleation model is validated and demonstrated in this dissertation. All of the macroscopic simulations were conducted in the commercial *MSC Marc* code, with a single *QUAD4* element with 4 integration points. The material properties considered for the micromechanics simulations are:

*Ductile matrix:* Young's modulus,  $E = 72$  GPa, Poisson's ratio  $\nu = 0.22$  and initial void volume fraction  $f_0 = 0.01$ . The post yield behavior for the matrix material without voids is governed by the yield curve shown in Figure 5.1. The yield stress is 175 MPa.

*Brittle SiC inclusions:* Young's modulus,  $E = 320$  GPa, Poisson's ratio  $\nu = 0.25$ .

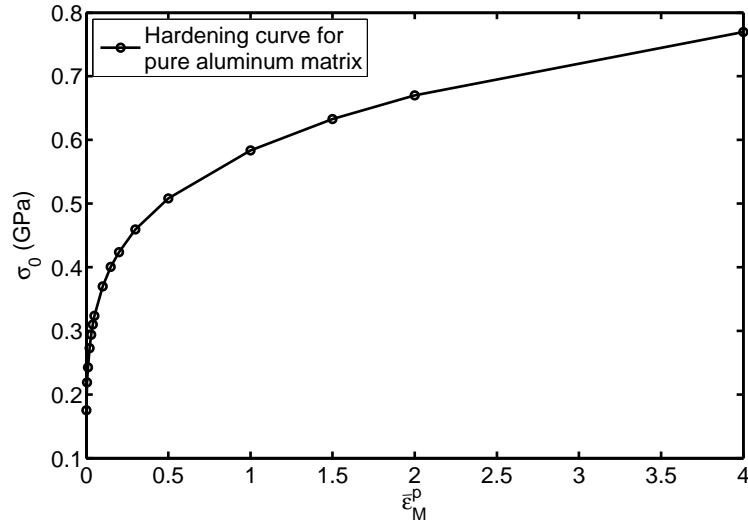


Figure 5.1: Hardening (stress-strain) curve for the aluminum matrix used for the micromechanics LE-VCFEM simulations of RVE 1 in Figure 4.3(a)

## 5.1 Viscoplastic response and void growth model

The RVE 1 shown in Figure 4.3(a), with 25 non-uniform elliptical inclusions of 10% volume fraction is used to validate the viscoplastic response of the macroscopic HCPD model, with and without void evolution. Four different micromechanics LE-VCFEM simulations with imposed shear loading, subject to different loading strain rates and initial void volume fraction  $f_0$  are conducted. The homogenized shear stress  $\Sigma_{xy}$  from the micromechanics simulations are compared to the macroscopic stress components, from HCPD simulations in Figure 5.2 and show excellent agreement. Homogenized results from the LE-VCFEM simulation of the same RVE 1 subject to a strain ratio of  $e_{xx} \neq 0 : e_{yy} = 0 : e_{xy} = 0$  at a strain rate of  $0.25 \text{ s}^{-1}$  along with the HCPD macroscopic stress components are show in Figure 5.3. From both the shear

and restricted tension tests, excellent agreement can be observed between the HCPD model and the homogenized micromechanics solutions.

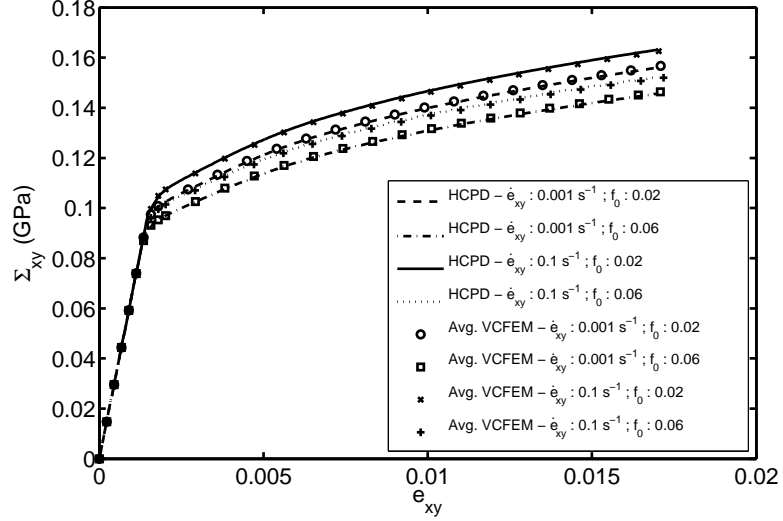


Figure 5.2: Macroscopic stress-strain response of the HCPD model and the homogenized micromechanical solutions for RVE 1 in Figure 4.3(a)

## 5.2 Void nucleation model

The void nucleation model is validated by simulating RVE 1 shown in Figure 4.3(a), with 25 non-uniform elliptical inclusions of 10% volume fraction. The plasticity parameters of this RVE is calibrated following the procedure described in Section 4.1 - 4.4. The nucleation parameters  $e_0$ ,  $m$ ,  $A$ ,  $B$  and  $C$  are calibrated following the procedure described in Section 4.5. The functional fit of the local strain rate dependent parameters  $e_0$  and  $m$  for the RVE 1 is shown in Figure 4.5 and 4.6. The major and minor axes of the ellipses describing the damage anisotropy parameters  $A$ ,  $B$  and  $C$  are given in Table 4.2. In order to validate the rate-dependent behavior

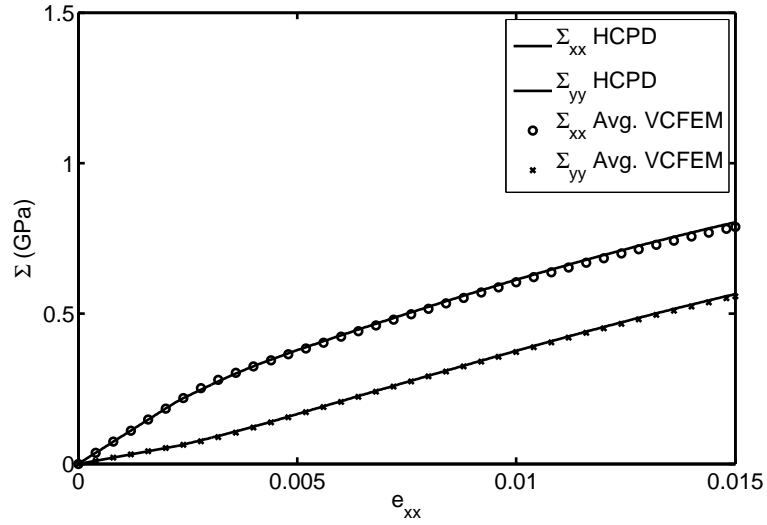


Figure 5.3: Macroscopic stress-strain response of the HCPD model and the homogenized micromechanical solution for RVE 1 in Figure 4.3(a) for strain ratio  $e_{xx} \neq 0 : e_{yy} = 0 : e_{xy} = 0$

of the nucleation model, four micromechanics LE-VCFEM simulations with RVE 1 are conducted, they are

1. Tension test in  $x$  direction with zero transverse strains ( $e_{xx} \neq 0 : e_{yy} = 0 : e_{xy} = 0$ ) at a loading strain rate of  $0.25 \text{ s}^{-1}$
2. Tension test in  $x$  direction with zero transverse strains ( $e_{xx} \neq 0 : e_{yy} = 0 : e_{xy} = 0$ ) at a loading strain rate of  $0.75 \text{ s}^{-1}$
3. Tension test in  $x$  direction with zero transverse strains ( $e_{xx} \neq 0 : e_{yy} = 0 : e_{xy} = 0$ ) at an initial loading strain rate of  $0.25 \text{ s}^{-1}$ , which is increased to  $0.75 \text{ s}^{-1}$  at 0.6% of the applied strain.

4. Tension test in  $x$  direction with zero transverse strains ( $e_{xx} \neq 0 : e_{yy} = 0 : e_{xy} = 0$ ) at an initial loading strain rate of  $0.75 \text{ s}^{-1}$ , which is decreased to  $0.25 \text{ s}^{-1}$  at 0.6% of the applied strain.

The homogenized responses of the micromechanics simulations stated above is compared with their respective macroscopic rate-dependent HCPD model simulation results in Figures 5.4 and 5.5 and show very good agreement. For both macroscopic and LE-VCFEM simulations, the Von-Mises stress is plotted as a function of the applied strain. The micromechanics simulations show discrete drops in stress due to the inclusions cracking, however the macroscopic model does not exhibit this behavior due to the continuous function used in the nucleation model. The evolution of the area fraction of the inclusions cracked  $\rho$  when there is an instantaneous change in strain rate from  $0.25 \text{ s}^{-1}$  to  $0.75 \text{ s}^{-1}$  is show in Figure 3.2 and  $\rho$  when there is an instantaneous change in strain rate from  $0.75 \text{ s}^{-1}$  to  $0.25 \text{ s}^{-1}$  is show in Figure 3.3. The factor  $\tilde{k}^*$  in Equation 3.19 takes care of the instantaneous change in local strain rate, accelerating and stalling the nucleation as required.

The ability of the nucleation model to capture material anisotropy in damage is validated by comparing the homogenized response from different micromechanics LE-VCFEM simulations subject to different loading conditions with their corresponding macroscopic HCPD response. Simulations are conducted for a number of applied macroscopic strain ratios ( $e_{xx} : e_{yy} : e_{xy}$ ) at an applied strain rate of  $0.1 \text{ s}^{-1}$ . The values of parameters  $A, B$  and  $C$  are obtained from the calibrated elliptical forms at the angle of principal strain corresponding to the local strains. The Comparison between the micromechanics result and the rate-dependent HCPD model results are shown in Figure 5.6 and show good agreement.

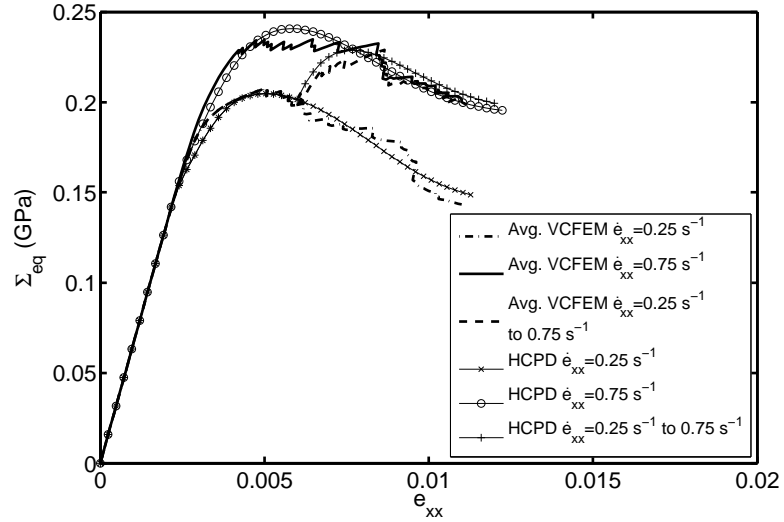


Figure 5.4: Comparison of macroscopic HCPD model simulation with the LE-VCFEM simulation of RVE 1 of Figure 4.3(a) subject to instantaneous change of strain rate from  $0.25 \text{ s}^{-1}$  to  $0.75 \text{ s}^{-1}$  at  $0.6\%$  applied strain.

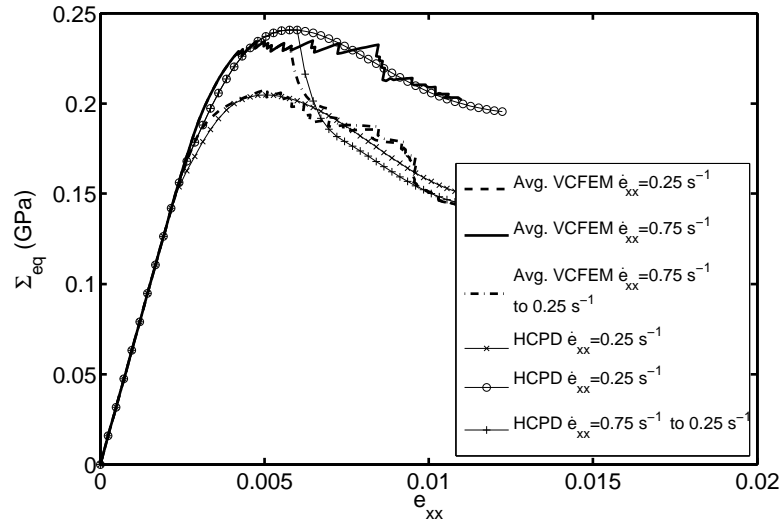


Figure 5.5: Comparison of macroscopic HCPD model simulation with the LE-VCFEM simulation of RVE 1 of Figure 4.3(a) subject to instantaneous change of strain rate from  $0.75 \text{ s}^{-1}$  to  $0.25 \text{ s}^{-1}$  at  $0.6\%$  applied strain.

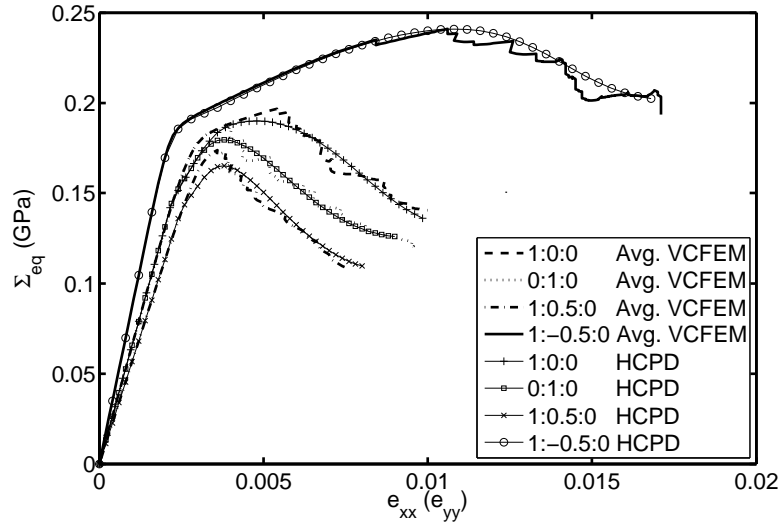


Figure 5.6: Macroscopic stress-strain response of the HCPD model and the homogenized LE-VCFEM solutions for RVE 1 in Figure 4.3(a) subject to different strain ratios  $e_{xx} : e_{yy} : e_{xy}$

For validating the elliptical forms of the nucleation parameters  $A, B$  and  $C$ , a number of LE-VCFEM simulations with different loading ratios ( $e_{xx} : e_{yy} : e_{xy} \neq 0$ ) were performed. The value of the parameter  $A$  is obtained from the ellipse shown in Figure 4.8 and from the homogenized micromechanics response, the parameter  $C$  is independently calibrated for different loading ratios. The independently calibrated values of the parameter  $C$  is plotted along with the elliptical form of  $C$  calibrated in Section 4.5 in Figure 5.7. From Figure 5.7, it is seen that the independently calibrated values are close to the elliptical form and thus validates the functional forms of the parameters  $A, B$  and  $C$ . Micromechanics simulations of RVE 1 for the two loading ratios  $e_{xx} = -1 : e_{yy} = 0.5 : e_{xy} = 0.5$  and  $e_{xx} = -1 : e_{yy} = 0.5 : e_{xy} = -0.5$  show no inclusion cracking. For these loading ratios, the value of  $A$  and  $C$  obtained from the ellipses calibrated in Section 4.5 used with Equation 3.14 and 3.17 gives a value of

zero for the area fraction of cracked inclusion  $\rho$ . Thus the anisotropy parameters are also capable of predicting loading conditions where no inclusion cracking happens.

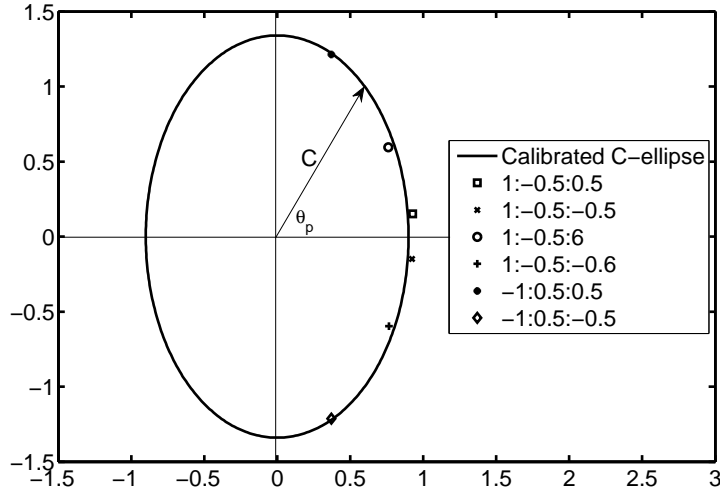


Figure 5.7: Parameter  $C$  for RVE 1 in Figure 4.3(a) along with the independently calibrated values of  $C$  for different strain ratios  $e_{xx} : e_{yy} = 0 : e_{xy} = 0$

### 5.3 Dual-stage nested homogenization

The rate-dependent HCPD model, with the void nucleation and growth part switched off is used for the macroscopic simulation of large secondary dendrite arm spacing or SDAS cast aluminum alloy microstructures in [2]. Microstructures of these alloys are characterized by extremely inhomogeneous distribution of inclusions along the dendrite cell boundaries. Traditional single-step homogenization methods are not suitable for this type of microstructure due to the size of the representative volume element (RVE) and the associated computations required for micromechanical analyses. To circumvent this limitation, two distinct statistically equivalent RVE's are

identified, corresponding to the inherent scales of inhomogeneity in the microstructure. The homogenization is performed in multiple stages for each of the RVE's identified. Asymptotic expansion homogenization (AEH) and Self consistent homogenization (SCH) are used in this method. Anisotropy and viscoplastic parameters in for the different scales are calibrated from homogenization of micro-variables for the different RVE's as described in Section 4.1 - 4.3. The uniqueness of the nested two-stage homogenization is that it enables evaluation of the overall homogenized model of the cast alloy from limited experimental data, but also material properties of constituents like inter-dendritic phase and pure aluminum matrix. The capabilities of the HCP model are demonstrated for a cast aluminum alloy AS7GU having a SDAS of  $30 \mu\text{.m}$  in [2].

## CHAPTER 6

### SUMMARY AND FUTURE WORK

#### 6.1 Summary

In this thesis, an accurate and computationally efficient rate-dependent homogenization based continuum plasticity damage model is developed for the macroscopic analysis of ductile fracture in heterogeneous porous ductile materials. The rate-dependent HCPD model is an extension of the model developed by Ghosh et al. [13] and follows the structure of an anisotropic Gursen-Tvergaard-Needleman elastoporous-plasticity model for ductile materials. Material anisotropy is determined by the morphology of the microstructure, evolution of plastic deformation and damage. This anisotropy in plastic behavior is modeled with a set of anisotropy parameters, which evolve as a function of the plastic work. The entire rate-dependent HCPD model is expressed in an evolving material principal coordinate system, in which the material remains orthotropic throughout the deformation history. All of the model parameters are calibrated from the homogenization of microstructural variables obtained from LE-VCFEM simulations of the RVE.

The model also incorporates a unique rate-dependent void nucleation criterion that is capable of effectively simulating the loss of load carrying capacity of heterogeneous materials that happens because of inclusion cracking and void growth. The

model incorporates the effects of loading strain rates on damage by using two parameters which are a function of the local strain rate. The nucleation model also incorporates the anisotropy in damage evolution using three parameters  $A$ ,  $B$  and  $C$ , which are rate-independent and can be calibrated at any loading strain rate. Numerical examples are conducted for a variety of loading conditions, like different strain rates, instantaneously varying strain rates and different loading ratios. In all the cases, the rate-dependent HCPD model results show excellent agreement with the homogenized micromechanics results. Above all the rate-dependent HCPD model has a huge advantage in terms of efficiency over explicit micromechanics simulations and hence is a very effective tool in making macroscopic damage predictions. These plasticity and nucleation capability is largely lacking in literature.

## 6.2 Future Work

Macroscopic analysis using the HCPD model has considerable efficiency advantage over explicit micromechanics simulations and hence the inclusion of such models in multi-scale framework for efficient analysis is inevitable. But it is also important to recognize the limitations of such homogenized models, especially the lack of accuracy and detail when simulating critical regions of microstructures containing cracks and highly localized damage evolution. Therefore implementation of the macroscopic rate-dependent HCPD model in a multi-scale framework, such as the one described in [28], followed by studies of error criterion and criterion for switching to lower scales is necessary.

## BIBLIOGRAPHY

- [1] S. Ghosh, D. M. Valiveti, S. J. Harris, and J. Boileau. A domain partitioning based pre-processor for multi-scale modeling of cast aluminum alloys. *Modelling Simul Mater Sci Eng*, 14:1363–1396, 2006.
- [2] D. Paquet, P. Dondeti, and S. Ghosh. Dual-stage nested homogenization for rate-dependent anisotropic elasto-plasticity model of dendritic cast aluminum alloys. *International Journal of Plasticity*, 2011.
- [3] Q. Wang. Microstructural effects on the tensile and fracture behaviour of aluminum casting alloys A356/357. *Metall Mater Trans Mech A*, 34:2887–2899, 2003.
- [4] J. Willis. Variational and related methods for the overall properties of composites. *Advan. Appl. Mech.*, 21:1–78, 1981.
- [5] P. Ponte Castaneda and P. Suquet. Nonlinear composites. *Advan. Appl. Mech.*, 34:171–302, 1998.
- [6] Z. Hashin. The elastic moduli of heterogeneous material. *J. Appl. Mech.*, 29:143–150, 1962.
- [7] T. Mori and K. Tanaka. Average stress in the matrix and average elastic energy of materials with misfitting inclusions. *Acta Metall.*, 21:571–574, 1973.
- [8] A. Benssousan, J.L. Lions, and G. Papanicoulau. *Asymptotic analysis for periodic structures*. North Holland, Amsterdam, 1978.
- [9] E. Sanchez-Palencia. *Non-homogeneous media and vibration theory, Lecture notes in Physics*. Springer-Verlag, Berlin Heidelberg, 1980.
- [10] S. Ghosh, K. Lee, and S. Moorthy. Multiple scale analysis of heterogeneous elastic structures using homogenization theory and Voronoi cell finite element model. *Int. J. Solids Struct.*, 32:27–62, 1995.

- [11] S. Ghosh, K. Lee, and S. Moorthy. Two scale analysis of heterogeneous elastic-plastic materials with asymptotic homogenization and Voronoi cell finite element model. *Comput. Methods. Appl. Mech. Engrg.*, 132:63–116, 1996.
- [12] S. Ghosh, K. Lee, and P. Raghavan. A multi-level computational model for multi-scale damage analysis in composite and porous materials. *Int. J. Solids Struct.*, 38:2335–2385, 2001.
- [13] S. Ghosh, J. Bai, and D. Paquet. Homogenization-based continuum plasticity-damage model for ductile failure of materials containing heterogeneities. *J Mech Phys Solids*, 57:1017–1044, 2009.
- [14] A.L. Gurson. Continuum Theory of Ductile Rupture by Void Nucleation and Growth: Part I. Yield Criteria and Flow Rule for Porous Ductile Media. *ASME J. Eng. Mater. Tech.*, 99:2–15, 1977.
- [15] C. Chu and A. Needleman. Void nucleation effects in biaxially stretched sheets. *J. Eng. Mater. Tech.*, 102:249–256, 1980.
- [16] V. Tvergaard. On localization in ductile materials containing voids. *Int. J. Frac.*, 18:237–251, 1982.
- [17] V. Tvergaard and A. Needleman. Analysis of cup-cone fracture in round tensile bar. *Acta Metall.*, 32:157–169, 1984.
- [18] D. Wang, J. Pan, and S. Liu. An anisotropic gurson yield criterion for porous ductile sheet metals with planar anisotropy. *Int. J. Damage Mech.*, 13:7–33, 2004.
- [19] A. Benzerga, J. Besson, and A. Pineau. Anisotropic ductile fracture part ii: theory. *Acta Metall.*, 52:4639–4650, 2004.
- [20] M. Garajeu and P. Suquet. Effective properties of porous ideally plastic or viscoplastic materials containing rigid particles. *J. Mech. Phys. Solids*, 45:873–902, 1997.
- [21] S. Swaminathan, S. Ghosh, and N. Pagano. Statistically equivalent representative volume elements for unidirectional composite microstructures: Part I - Without damage. *J Compos Mater*, 40:583–604, 2006.
- [22] S. Swaminathan and S. Ghosh. Statistically equivalent representative volume elements for unidirectional composite microstructures: Part II - With damage. *J Compos Mater*, 40:605–621, 2006.

- [23] R. Pyrz. Quantitative description of the microstructure of composites: I. Morphology of unidirectional composite systems. *Compos Sci Technol*, 50:197–208, 1994.
- [24] S. Ghosh and S. Mukhopadhyay. A two dimensional automatic mesh generator for finite element analysis of randomly dispersed composites. *Comput Struct*, 41:245–256, 1991.
- [25] P. Raghavan and S. Ghosh. Adaptive multiscale modeling of composite materials. *Comp Model Engng Sci*, 5(2):151–170, 2004.
- [26] P. Raghavan and S. Ghosh. Concurrent multi-scale analysis of elastic composites by a multi-level computational model. *Comput Meth Appl Mech Engng*, 193(6-8):497–538, 2004.
- [27] P. Raghavan and S. Ghosh. A continuum damage mechanics model for unidirectional composites undergoing interfacial debonding. *Mech. Mater.*, 37:955–979, 2005.
- [28] S. Ghosh, J. Bai, and P. Raghavan. Concurrent multi-level model for damage evolution in microstructurally debonding composites. *Mech. Mater.*, 39:241–266, 2007.
- [29] S. Moorthy and S. Ghosh. Adaptivity and convergence in the Voronoi cell finite element model for analyzing heterogeneous materials. *Comput Method Appl Mech Engng*, 185:37–74, 2000.
- [30] S. Moorthy and S. Ghosh. A Voronoi cell finite element model for particle cracking in elastic-plastic composite materials. *Comput Method Appl Mech Engng*, 151:377–400, 1998.
- [31] C. Hu and S. Ghosh. Locally enhanced voronoi cell finite element model (levcfem) for simulating evolving fracture in ductile microstructures containing inclusions. *Inter. Jour. Numer. Meth. Engng.*, 76(12):1955–1992, 2008.
- [32] D. Paquet and S. Ghosh. Microstructural effects on ductile fracture in heterogeneous materials. Part I: Sensitivity analysis with LE-VCFEM. *Eng Fract Mech*, page doi:10.1016/j.engfracmech.2010.07.009, 2010.
- [33] D. Paquet and S. Ghosh. Microstructural effects on ductile fracture in heterogeneous materials. Part II: Application to cast aluminum microstructures. *Eng Fract Mech*, page doi:10.1016/j.engfracmech.2010.07.010, 2010.
- [34] P. Perzyna. Fundamental problems in viscoplasticity. *Adv Appl Mech*, 9:243–377, 1966.

- [35] R. Hill. On constitutive macro-variables for heterogenous solids at finite strain. *Proc Roy Soc Lond*, 326:131–147, 1972.
- [36] R. Hill. A theory of yielding and plastic flow of anisotropic metals. *Proc Roy Soc A - Math Phy*, 193:281–297, 1948.
- [37] T. Beytschko, W.K. Liu, and B. Moran. *Nonlinear Finite Elements for Continua and Structures*. Wiley, England, 2000.